

Andrés Ricardo Valdez

**On Lattice Boltzmann Method for Solving Fluid-Structure Interaction
Problems**

Dissertação apresentada ao Programa de Pós-graduação em Modelagem Computacional, da Universidade Federal de Juiz de Fora como requisito parcial à obtenção do grau de Mestre em Modelagem Computacional.

Orientador: Prof. D.Sc. Bernardo Martins Rocha

Coorientador: Prof. D.Sc. Iury Higor Aguiar da Igreja

Juiz de Fora

2017

Valdez, Andrés Ricardo

On Lattice Boltzmann Method for Solving Fluid-Structure Interaction Problems/Andrés Ricardo Valdez. – Juiz de Fora: UFJF/MMC, 2017.

XIV, 74 p. 29, 7cm.

Orientador: Bernardo Martins Rocha

Coorientador: Iury Higor Aguiar da Igreja

Dissertação (mestrado) – UFJF/MMC/Programa de Modelagem Computacional, 2017.

Bibliography: p. 67 – 73.

1. Métodos Variacionais. 2. Escoamento complexo. 3. Interação Fluido-Estrutura. 4. Método de Lattice Boltzmann. 5. Método de Fronteira Imersa. I. Rocha, Bernardo Martins et al.. II. Universidade Federal de Juiz de Fora, MMC, Programa de Modelagem Computacional.

Andrés Ricardo Valdez

On Lattice Boltzmann Method for solving Fluid-Structure Interaction
Problems

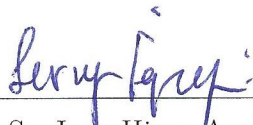
Dissertação apresentada ao Programa de Pós-graduação em Modelagem Computacional, da Universidade Federal de Juiz de Fora como requisito parcial à obtenção do grau de Mestre em Modelagem Computacional.

Aprovada em 18 de Setembro de 2017.

BANCA EXAMINADORA



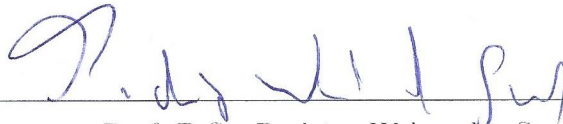
Prof. D.Sc. Bernardo Martins Rocha - Orientador
Universidade Federal de Juiz de Fora



Prof. D.Sc. Iury Higor Aguiar da Igreja - Coorientador
Universidade Federal de Juiz de Fora



Prof. D.Sc. José Karam Filho
Laboratório Nacional de Computação Científica



Prof. D.Sc. Rodrigo Weber dos Santos
Universidade Federal de Juiz de Fora

*Dedicated to everybody who
trusted me.
Specially those who still trust me.*

ACKNOWLEDGMENTS

This dissertation represents the junction of time, and unmeasurable human resources. In first place I would like to highlight the patience of my *advisory council* Bernardo and Iury they both have provided me academic guidance with enormous simplicity. Therefore I would like to thank to both of them not only for the academic advice but for their friendship. In less than one year they have helped me to hand out material for publishing in academic journals, and conference proceedings and a Master's Dissertation.

I also would like to thank the comments and corrections pointed out by the examination board, specially those ones coming from professors Rodrigo Weber dos Santos and José Karam Filho. Every comment, suggestion they made exalts the value of this Dissertation, allowing me to improve my background knowledge.

In what concerns colleagues and friends I would like to thank the predisposition of Lucão and Ruy, from the UFJF PhD graduate program. From my previous stage at the *overlook* I would like to thank the friendship demonstrated by Felipe, Leandro, Aaron, Secis, Tharso, Leonardo, Allan, and Alonso. I also would like to thank the provided help coming from Renata, Samantha and Rafael (sometimes I speak strange but they managed to understand me).

I would like to thank my parents Marta and Hugo and my brother Felipe for their constant support, and dedicate this work to my wife Anna. Everything results viable if there is someone waiting you with a smile at home.

To conclude I must acknowledge the economic resources provided by FAPEMIG and UFJF to develop this Master's Dissertation.

ANDRÉS RICARDO VALDEZ

SEPTEMBER 2017. JUIZ DE FORA MG

*Andrés tenés dos alternativas,
Estudiar o estudiar.*

— Mamá

RESUMO

Neste trabalho são apresentados aspectos de modelagem computacional para o estudo de Interação Fluido-Estrutura (FSI). Numericamente, o Método de Lattice Boltzmann (LBM) é usado para resolver a mecânica dos fluidos, em particular as equações de Navier-Stokes incompressíveis. Neste contexto, são abordados problemas de escoamentos complexos, caracterizado pela presença de obstáculos. A imposição das restrições na interface fluido-sólido é feita utilizando princípios variacionais, empregando o Princípio de Balanço de Potências Virtuais (PVPB) para obter as equações de Euler-Lagrange. Esta metodologia permite determinar as dependências entre carregamentos cinematicamente compatíveis e o estado mecânico adotado. Neste sentido, as condições de interface fluido-sólido são abordadas pelo Método de Fronteira Imersa (IBM) visando técnicas computacionais de baixo custo. A metodologia IBM trata o equilíbrio das equações na interface fluido-sólido através da interpolação entre os nós Lagrangianos (sólidos) e os nós Eulerianos (fluidos). Neste contexto, uma modificação desta estratégia que fornece soluções mais precisas é estudada. Para mostrar as capacidades do acoplamento LBM-IBM são apresentados vários experimentos computacionais que demonstram grande fidelidade entre as soluções obtidas e as soluções disponíveis na literatura.

Palavras-chave: Métodos Variacionais. Escoamento complexo. Interação Fluido-Estrutura. Método de Lattice Boltzmann. Método de Fronteira Imersa.

ABSTRACT

This work presents computational modeling aspects for studying Fluid-Structure Interaction (FSI). The Lattice Boltzmann Method (LBM) is employed to solve the fluid mechanics considering the incompressible Navier-Stokes equations. The flows studied are complex due to the presence of arbitrary shaped obstacles. The obstacles alters the bulk flow adding complexity to the analysis. In this work the Euler-Lagrange equations are obtained employing the Principle of Virtual Power Balance (PVPB). Consequently, the functional dependencies between the mechanical state and every kinematic compatible loadings are established employing variational arguments. This modeling technique allows to study the fluid-solid boundary constraint. In this context the fluid-solid interface is handled employing the Immersed Boundary Method (IBM). The IBM deals with the fluid-solid interface equilibrium equations performing an interpolation of forces between Lagrangian nodes (solid domain) and Eulerian Lattice grid (fluid domain). In this work a different version of this methodology is studied that allows to obtain more accurate solutions. To show the capabilities of the implemented LBM-IBM solver several experiments are done showing the agreement with the benchmarks results available in literature.

Keywords: Variational Methods. Complex Fluid Flow. Fluid-Structure Interaction. Lattice Boltzmann Method. Immersed Boundary Method.

CONTENTS

List of Figures	11
List of Tables	13
List of Symbols	14
1 INTRODUCTION	15
1.1 Motivation	15
1.2 Objectives and contributions of the work	18
1.2.1 Methodology to model FSI: Euler-Lagrange equations	18
1.2.2 Numerical solutions: LBM-IBM	19
1.3 Dissertation's structure	19
2 CONTINUUM MECHANICS MODELING FRAMEWORK	20
2.1 Notation	20
2.2 Kinematics	21
2.3 Motion Actions: Kinematic Constraints	22
2.4 Power Duality	22
2.5 Virtual Power Balance in Continuum Mechanics	23
2.6 Unconstrained mechanical state manifolds problem	25
2.7 Fluid Mechanics Variational Framework	26
2.7.1 Fluid mechanics mechanical state	26
2.7.2 Fluid mechanics measures of expended power	27
2.7.3 Fluid mechanics Virtual Power Balance	27
3 NUMERICAL METHODS	30
3.1 Introduction	30
3.2 Lattice Boltzmann Method (LBM)	31
3.2.1 Boltzmann's Equation	31
3.2.2 LBM	32
3.2.3 Equilibrium Distribution	33

3.2.4	<i>The D2Q9 Lattice array</i>	34
3.2.5	<i>Boundary Conditions</i>	35
3.3	Fluid-structure interaction	36
3.3.1	<i>The Forcing Method</i>	36
3.3.2	<i>Immersed Boundary Method</i>	38
3.3.3	<i>IBM for rigid obstacles</i>	41
3.3.4	<i>Parameters for fluid-structure interaction simulations</i>	42
4	NUMERICAL RESULTS	44
4.1	Kovaszny problem	44
4.2	Flows with rigid obstacles	46
4.2.1	<i>Flow around a spinning circle</i>	46
4.2.2	<i>Turek's Benchmark</i>	48
4.2.3	<i>Flow around a cylinder</i>	52
4.2.4	<i>The von Karman Vortex Street</i>	55
4.2.5	<i>Flow Around a Square Cylinder</i>	59
4.2.6	<i>Flow around a shield</i>	60
5	CONCLUDING REMARKS	63
5.1	Limitations and Future Works	65
5.2	Academic Contributions	65
	Bibliography	67

List of Figures

1.1	Tacoma Narrows bridge collapse	16
1.2	<i>Stent</i> function preventing <i>stenosis</i> , adapted from [14]	16
1.3	Adapted from Mercedes Benz [4].	17
2.1	Principal elements involved in the PVPB.	24
3.1	The D2Q9 Lattice array.	34
3.2	Physical situation (left) and forcing method approach (right), the affected Lattices are highlighted in blue.	38
3.3	Physical situation (left) and IBM approach (right) with Lagrangian nodes highlighted in red.	39
3.4	IBM interpolation kernel. The interface nodes are colored with red, and the affected Lattice's nodes are highlighted with blue.	40
4.1	Velocity field for the Kovasznay flow.	45
4.2	Comparison between the classic IBM scheme (3.23) vs. the enhanced IBM scheme (3.24).	46
4.3	Flow patterns analysis considering $R_E = 20$. The contour maps corresponds to the distribution of the $\boldsymbol{\gamma}(\mathbf{r}, t)$ vector field.	47
4.4	Drag and lift forces for different Reynolds numbers.	48
4.5	Geometry of the flow around a cylinder, the geometry was re-scaled to Lattice units.	48
4.6	Available solutions handed out for <i>Test case 2D-1 (steady)</i> , the solutions highlighted in red corresponds to the research group that employed a LBM-BGK CFD solver. Adapted from [59].	50
4.7	Forcing method vs IBM, drag and lift analysis.	51

4.8	Velocity contour maps comparison. (a) forcing method and (b) IBM. . . .	52
4.9	Geometry of the flow around a cylinder.	53
4.10	Flow around a circular cylinder: Velocity field considering different Reynolds numbers.	54
4.11	Drag coefficients at different Reynolds numbers.	55
4.12	Geometry of the flow around a cylinder.	55
4.13	Vortex principal separation modes. Adapted from [61].	56
4.14	Velocity field.	57
4.15	u_x field variations during the simulations.	58
4.16	u_y field variations during the simulations.	58
4.17	Density variations during the simulations.	59
4.18	Geometry of the flow around a square cylinder.	59
4.19	Drag coefficients at different Reynolds numbers.	60
4.20	Velocity field for the case with Reynolds 50.	60
4.21	Geometry of the flow around a planar shield.	61
4.22	Velocity field for different Reynolds numbers.	62

List of Tables

3.1	IBM coefficients used in this work.	42
3.2	Equilibrium distribution optimal coefficients to ensure stability.	42
4.1	History convergence for Kovasznay Flow.	45

List of Symbols

u, v	Scalar functions
\mathbf{u}, \mathbf{v}	Vectorial functions
nd	Number of spatial dimensions, (in this work fixed in 2)
\mathbf{H}^m	Hilbert vectorial space regular enough till the m derivative
$(\cdot; \cdot)$	Inner product
$\langle \cdot; \cdot \rangle$	Dual- <i>like</i> product
Ω	Lipschitz domain
$\partial\Omega, \Gamma$	Regular enough boundaries
$\text{Lin}(\cdot, \cdot)$	Space of linear maps
$\text{Kin } \mathcal{U}$	Kinematic admissible manifold
$\text{Var } \mathcal{U}$	Kinematic admissible vectorial space
$\mathbb{T}, \mathbb{D}, \mathbb{I}$	Second order tensors
$(\cdot)^*$	Adjoint quantity of the vector, set (\cdot)
$(\cdot)^T$	Transpose quantity of the vector, tensor (\cdot)
$(\hat{\cdot})$	Admissible variation of the vector, set (\cdot)
$\nabla(\cdot)$	Gradient of the scalar, vectorial field (\cdot)
$\text{div}(\cdot)$	Divergent of the vectorial field (\cdot)
$(\dot{\cdot}), (\ddot{\cdot})$	First and second time derivative of the scalar, vectorial field (\cdot) , respectively

1 INTRODUCTION

1.1 Motivation

Coupled problems like Fluid-Structure Interaction (FSI) are of special interest in many engineering areas. The flow bounded by solid structures is possible to be solved knowing the shape and position of the solid domain; as a consequence of this interaction the fluid exerts on the solid reactive forces. In this context it is important to understand:

- a) the magnitude of the forces that the fluid exerts on the solid domain;
- b) the nature of those forces: are they transient or instantaneous or quasi-static?
- c) and, finally: how the solid domain behaves in presence of fluid forces?

It is important to understand the nature of the forces that the fluid prints over the solid domain, to describe common effects like aircraft's fluttering, sock's flapping, airbag's inflation, blood flow and arterial dynamics, among others. Basically the equilibrium of forces between solid and fluid domains can be characterized in three ways: (i) unstable, (ii) quasi-stable and (iii) stable. In this context a stable equilibrium corresponds to any state of motion that remains constant during the motion. On the other hand, if the state of motion addresses changes, in absence of forces, the equilibrium is no longer stable; allowing to describe unstable and quasi-stable equilibriums.

Therefore, studies considering FSI phenomena are important to better understand catastrophic events like the falling down of the *Tacoma Narrows Bridge* (see Figure 1.1); or for the understanding on how to design efficient prosthetic devices such as stents for biomedical engineering, as shown in Figure 1.2.

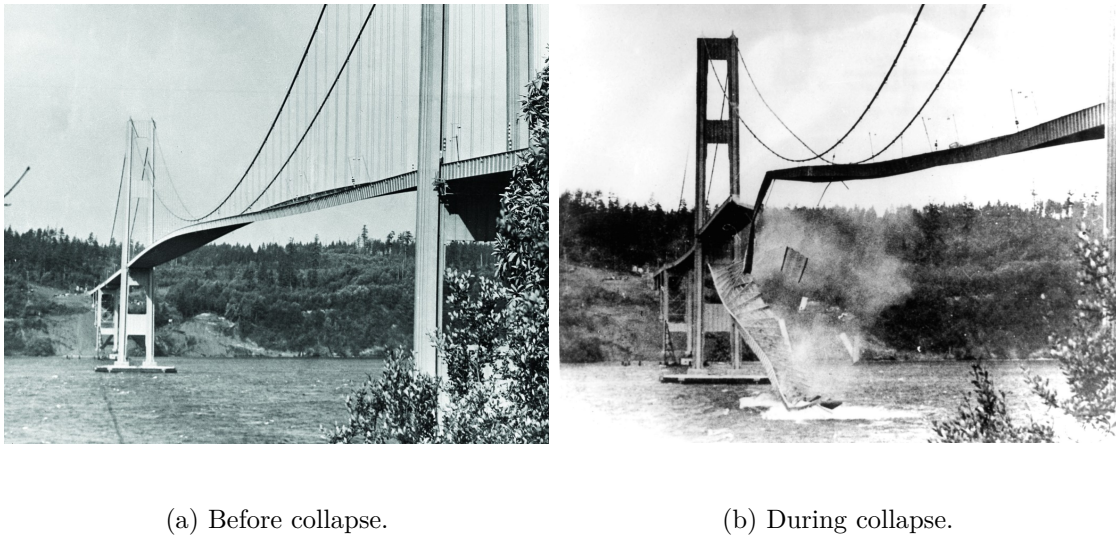


Figure 1.1: Tacoma Narrows bridge collapse

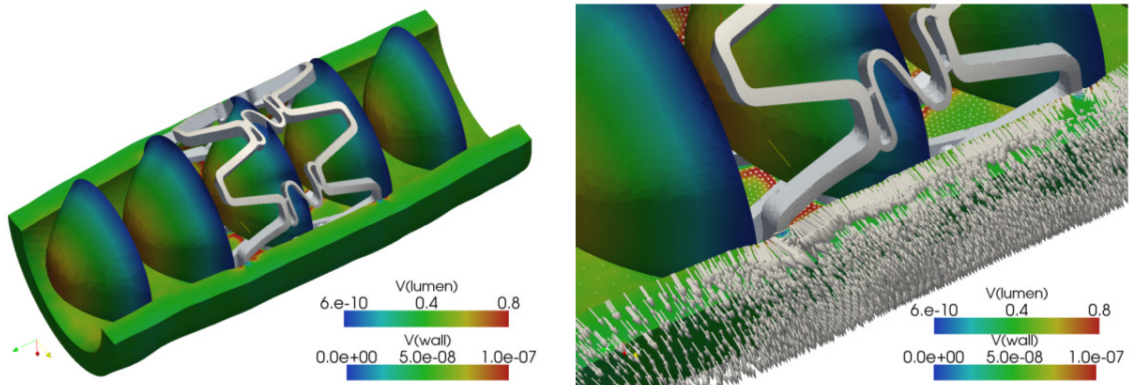


Figure 1.2: *Stent* function preventing *stenosis*, adapted from [14]

As reported by Maugin [33, 34, 35] over the last centuries there has been a compelling need to reproduce the complex behavior of nature with coupled phenomena. In this context, the FSI problems experienced a remarkable evolution of knowledge employing experimental analysis. Among the several analysis, we can highlight the wind tunnels that are often used to evaluate the performance of a prototype when subjected to aerodynamics forces, see Figure 1.3.



Figure 1.3: Adapted from Mercedes Benz [4].

The use of experimental techniques like analysis with a wind tunnel is helpful to understand the behavior of a prototype. Nevertheless, the use of the wind tunnel does not give hints for optimizing the prototype and also does not give information to forecast the behavior of the prototype when subjected to different forces or scenarios. In some cases, the experiment is difficult to characterize, because it is entangled to determine a reliable technique to measure non-dimensional numbers like: Reynolds number¹, Mach number², and Froude number³. As mentioned by Lönher [31] the accurate control of these three number is often complicated, specially when considering events that involves the destruction of the prototype or the wind tunnel itself or human casualties. For example the development of (nuclear) bombs does not allows to use wind tunnels, back in the 1940's and 1950's nuclear tests where often used and considered necessary to validate new designs and combination of gunpowder. At the present time computational mechanics allows to understand the "satisfactory" combination of gunpowder and other materials to provoke the destruction of a desired target, without detonating a single bomb.

The present challenges for computational mechanics concern topics like:

- the partial replacement of experimental analysis with numerical simulations,
- analyze the results coming from numerical simulation to forecast dependencies,
- reduce the cost of experiments to the minimum.

¹The Reynolds number is the ratio of inertial forces towards viscous forces.

²The Mach number is the ratio of the velocity past an obstacle refereed to the velocity of sound.

³The Froude number is the ratio of the flow inertia towards the external forces.

In this context the *computational mechanics* is presented as an alternative to fill-in the gaps left by experimental analysis when modeling complex situations like: bio-medical devices design like the one shown with Figure 1.2. Recently, computational mechanics has provided answers towards the characterization of blood flow considering bifurcations, as reported by Artoli *et al.* [2]. In [2] the flow faces changes on the domain, modifying the distribution of the velocity vector field and the shear stresses. In particular, considering computational Hemodynamics, the works of Artoli [1, 3] analyzes the possibilities to model blood flow in domains reconstructed with *Computational Tomography*. Specially in [3], the focus is put on studying the process of white blood cell margination. The margination of a blood cell refers to the state of equilibrium of a cell immersed in the blood flow (The cell can follow the blood stream and roll). These analysis allow to understand several process like immunity decay towards the presence of infections. Inflammation of an infected area is the result of white blood cell's margination, coming from the blood vessel and infiltrating in to the damaged tissue.

1.2 Objectives and contributions of the work

The main contribution of this work is to establish a methodology to simulate incompressible flows considering the inclusion of arbitrary-shaped obstacles. For this we present a self-consistent technique to obtain the Euler-Lagrange equations. And afterwards solve them employing the Lattice Boltzmann Methods coupled to the Immersed Boundary Method. To determine the robustness of the methodology we show several simulations highlighting the agreement between the reference's gold standards and our results.

1.2.1 Methodology to model FSI: Euler-Lagrange equations

In order to model the behavior of fluid flow considering complex conditions, in this section some important continuum mechanics concepts are presented. The procedure to formulate the problem is the result of: (i) kinematic admissibility, (ii) mathematical duality and, (iii) the Principle of Virtual Power Balance (PVPB).

This modeling technique has been applied showing the equivalence between the PVPB and the Euler-Lagrange equations corresponding to coupled problems in the works of [12,

20, 32], concerning physics like: solid mechanics, fluid mechanics, electro-magnetics, dissipative mechanics, among others. Thus, the PVPB has been used as an alternative method to model coupled physics. The validity of this method was analyzed in [21, 36] highlighting the modeling of complex physics. Moreover, the Constitutive modeling has used the PVPB approach to characterize the kinematic compatible loadings (external and internal loadings) [17, 48, 43].

1.2.2 Numerical solutions: LBM-IBM

Once the Euler-Lagrange equations governing the complex fluid flow are derived, a numerical method has to be applied in order to obtain approximate solutions. To this, we employ the Lattice Boltzmann Method (LBM) due to the successfully to obtain accurate solutions for the incompressible Navier-Stokes equations [11, 24, 40]. The method is very attractive from the computational point of view and when combined with other methods offers an interesting approach for FSI problems, as will be shown.

To solve realistic problems like the inclusion of arbitrary-shaped obstacles in the flow we couple LBM with the IBM. The IBM is a computational option to refine the grid in order to achieve an accurate representation of complex geometries, that can be viewed in works of Peskin [44, 45, 47, 37, 46]. However, in this work a different scheme for dealing with rigid obstacles is discussed, validated and compared with classical approach by available benchmarks in the literature.

1.3 Dissertation's structure

This work is organized as follows: a methodology for obtaining the Euler-Lagrange equations that models obstructed fluid flow is shown in chapter 2. In chapter 3, the numerical methodologies are presented and analyzed to obtain the solution of the corresponding boundary value problem, featuring methods like LBM and IBM. A combination of these numerical techniques are validated and tested in chapter 4, demonstrating the versatility and robustness of the computational implementation. Finally, future works, conclusion and remarks are adressed in chapter 5.

2 CONTINUUM MECHANICS

MODELING FRAMEWORK

This chapter presents a methodology to study functional dependencies between generalized loadings (stresses, body forces, surface tractions) and generalized displacements (displacements, velocities, strain rates). The Euler-Lagrange equations are responsible for characterizing kinematic compatible loadings with the adopted kinematics. In this work the Euler-Lagrange equations are obtained following the three invariant steps:

- i) define convenient kinematics. The kinematics is defined characterizing the regularity and the appropriate boundary restrictions to model the problem;
- ii) define dual-like power measures. The dual-like measures represents the power expended to perform changes on the kinematic state variables; and
- iii) evoke the PVPB, to characterize the equilibrium.

The consequences of this procedure are equivalent to consider the balance of *momentum* as reported by Truesdell [56, 58, 55] and Germain [21]. For example, if needed to evaluate the weight of an object, firstly it is required to provide a vertical displacement degree of freedom, acknowledging a rigid motion. Secondly, it is necessary to measure the exerted virtual power. Finally the expression of the virtual power balance resumes the fact that the density of the object times gravity is the weight of the object.

For the scope of continuum mechanics the virtual power balance has been analyzed in the following works [5, 6, 42, 54]. For certain cases like linear elasticity, creeping flow mechanics, among others, the expressions obtained employing the PVPB are equivalent to find the conditions that minimizes a particular cost functional, as can be viewed in [15, 51, 41]

2.1 Notation

In this work, scalar fields are defined as u, v and bold symbols are used to denote the vector fields \mathbf{u}, \mathbf{v} . Let $\Omega \subset \mathbb{R}^{nd}$, $nd = \{2, 3\}$, be a bounded domain with a Lipschitz

boundary $\partial\Omega$. In this domain we set

$$L^2(\Omega) \equiv \left\{ v \in \Omega : \int_{\Omega} |v|^2 \, d\Omega < \infty \right\},$$

as the space of square integrable functions, and

$$H^1(\Omega) \equiv \left\{ v \in L^2(\Omega) : \nabla v \in L^2(\Omega) \right\},$$

where ∇ denotes the gradient operator.

For vectorial fields the following generalization is valid:

$$\begin{cases} \mathbf{L}^2(\Omega) &= (L^2(\Omega))^{nd}, \\ \mathbf{H}^1(\Omega) &= (H^1(\Omega))^{nd}. \end{cases}$$

As reported by Taroco [54] and Berdichevsky [5, 6] for functional spaces, the *inner product* is introduced as $(\mathbf{u}; \mathbf{v}) = \mathbf{u} \cdot \mathbf{v}$. The *Mathematical Duality* is represented by $\langle \mathbf{u}; \mathbf{v} \rangle_{\mathcal{U}^* \times \mathcal{U}} \implies (\mathbf{u}; \mathbf{v})$, where $\mathbf{u} \in \mathcal{U}^*$ and $\mathbf{v} \in \mathcal{U}$, with the subset \mathcal{U}^* being the dual subset of \mathcal{U} .

2.2 Kinematics

For the purposes of this work a general description for a motion is done by defining a *mechanical state* field denoted by \mathbf{E} . Thus, for any $\mathbf{x} \in \Omega$, the generalized mechanical state yields the following definition:

$$\begin{aligned} \mathbf{E} : \Omega &\rightarrow \mathbb{R}^{nd}, \\ \mathbf{x} &\mapsto \mathbf{E}. \end{aligned} \tag{2.1}$$

For the scope of this analysis, the first gradient modeling scheme is employed. The first gradient models the balance between generalized forces and generalized stresses, this theory is explained in the works of [5, 6, 54]. As a consequence of the first gradient scheme it is necessary to define a generalized motion action $\mathbb{D}(\mathbf{E})$ as:

$$\begin{aligned}\mathbb{D} &: \text{Lin}(\mathbb{R}^{nd}, \mathbb{R}^{nd}), \\ \mathbf{E} &\mapsto \mathbb{D}(\mathbf{E}) = \nabla \mathbf{E},\end{aligned}\tag{2.2}$$

where $\text{Lin}(\mathbb{R}^{nd}, \mathbb{R}^{nd})$ represents the space of linear functions with support and range on the vectorial space \mathbb{R}^{nd} .

2.3 Motion Actions: Kinematic Constraints

The mechanical state functional space is characterized taking into account: well-posed regularity, Dirichlet's boundary conditions (often known as *essential boundary conditions*) and if needed distributed constraints. For this analysis the mechanical state lies on the following manifold:

$$\text{Kin } \mathcal{U} = \{ \mathbf{w} \in \mathbf{H}^1(\Omega) : \mathbf{w}|_{\partial\Omega_D} = \mathbf{E}_D, \mathcal{G}(\mathbf{w}) = 0 \in \Omega \},\tag{2.3}$$

where $\partial\Omega_D$ denotes the boundary with prescribed values for the mechanical state \mathbf{E} , in this case $\mathbf{E} - \mathbf{E}_D = \mathbf{0}$ and $\mathcal{G}(\mathbf{w}) = 0$ represent a distributed restriction in Ω . It is also possible to characterize the subspace $\text{Var } \mathcal{U}$ of kinematically admissible variations as follows:

$$\text{Var } \mathcal{U} = \{ \mathbf{u}_1 - \mathbf{u}_2 \in \text{Var } \mathcal{U} : \mathbf{u}_1, \mathbf{u}_2 \in \text{Kin } \mathcal{U} \}.\tag{2.4}$$

2.4 Power Duality

The kinematic admissible manifold (2.3) takes into account measures of the mechanical state and its gradient. In this context two different powers are recognized:

- Internal Power (P^{int}). Addresses the expended power used to perform changes in the strain rate tensor. The internal power is considered to be a linear and continuous functional defined over the $\mathbb{D}(\mathbf{E})$, which can be mathematically expressed as

$$P^{\text{int}} : \mathbb{R}^{nd*} \times \mathbb{R}^{nd} \rightarrow \mathbb{R},$$

where the space \mathbb{R}^{nd*} is the dual space of \mathbb{R}^{nd} . Using the Riesz representation theorem [54], the linear operator has the unique representation,

$$P^{\text{int}}(\mathbb{D}(\mathbf{E})) = \langle \mathbb{A}; \mathbb{D}(\mathbf{E}) \rangle_{\mathbb{R}^{nd*} \times \mathbb{R}^{nd}}.$$

The new element $\mathbb{A} \in \text{Lin}(\mathbb{R}^{nd}, \mathbb{R}^{nd})$ is called stress tensor.

- External Power (P^{ext}). Addresses the expended power used to perform changes in the mechanical state vector. The external power is considered to be a linear and continuous functional defined over the mechanical state, which can be mathematically expressed as

$$P^{\text{ext}} : \mathbb{R}^{nd*} \times \mathbb{R}^{nd} \rightarrow \mathbb{R}.$$

Using Riesz representation theorem, the linear operator has unique representation,

$$P^{\text{ext}}(\mathbf{E}) = \langle \mathbf{f}; \mathbf{E} \rangle_{\mathbb{R}^{nd*} \times \mathbb{R}^{nd}},$$

where $\mathbf{f} \in \mathbb{R}^{nd*}$ represents a generalized external load.

These duality products must satisfy the following properties [54]:

$$\begin{aligned} \langle \mathbb{A}; \mathbb{D}(\mathbf{E}) \rangle_{\mathbb{R}^{nd*} \times \mathbb{R}^{nd}} &= 0, & \forall \mathbb{D}(\mathbf{E}) \in \mathbb{R}^{nd} &\Rightarrow \mathbb{A} = \mathbf{0}, \\ \langle \mathbb{A}; \mathbb{D}(\mathbf{E}) \rangle_{\mathbb{R}^{nd*} \times \mathbb{R}^{nd}} &= 0, & \forall \mathbb{A} \in \mathbb{R}^{nd*} &\Rightarrow \mathbb{D}(\mathbf{E}) = \mathbf{0}, \\ \langle \mathbf{f}; \mathbf{E} \rangle_{\mathbb{R}^{nd*} \times \mathbb{R}^{nd}} &= 0, & \forall \mathbf{E} \in \mathbb{R}^{nd} &\Rightarrow \mathbf{f} = \mathbf{0}, \\ \langle \mathbf{f}; \mathbf{E} \rangle_{\mathbb{R}^{nd*} \times \mathbb{R}^{nd}} &= 0, & \forall \mathbf{f} \in \mathbb{R}^{nd*} &\Rightarrow \mathbf{E} = \mathbf{0}. \end{aligned}$$

2.5 Virtual Power Balance in Continuum Mechanics

To model continuum mechanics problems in this work the balance of virtual power is used, which is equivalent to model the problem considering the balance of *momentum* balance of *mass* and other constraints, as reported by Germain [20, 21]. To use the virtual power balance the following axiom is stated:

Axiom 2.1 (Principle of Virtual Power Balance (PVPB)). *Let a system Ω be in equilibrium*

with respect to a given frame of reference; then, in any virtual motion, the virtual power of all the internal forces and external forces acting on Ω is null, i.e.:

$$\begin{aligned} P^{\text{int}}(\mathbb{D}(\hat{\mathbf{E}})) + P^{\text{ext}}(\hat{\mathbf{E}}) &= \langle \mathbb{A}; \mathbb{D}(\hat{\mathbf{E}}) \rangle_{\mathbb{R}^{nd^*} \times \mathbb{R}^{nd}} + \langle \mathbf{f}; \hat{\mathbf{E}} \rangle_{\mathbb{R}^{nd^*} \times \mathbb{R}^{nd}} \\ &= 0 \quad \forall \hat{\mathbf{E}} \in \text{Var } \mathcal{U}. \end{aligned} \quad (2.5)$$

The PVPB itself retrieves a mathematical expression for the concept of *equilibrium* which is used to characterize the kinematic compatible loadings $\mathbb{A}(\mathbf{E}) \in \mathbb{R}^{nd^*}$ and $\mathbf{f} \in \mathbb{R}^{nd^*}$. For this objective, the adjoint transformation results particularly useful for this characterization, as mentioned in [41, 54]. Thus, the inner power functional can be rewritten employing the adjoint transformation as follows:

$$\langle \mathbb{A}; \mathbb{D}(\hat{\mathbf{E}}) \rangle_{\mathbb{R}^{nd^*} \times \mathbb{R}^{nd}} = \langle \mathbb{D}^* \mathbb{A}; \hat{\mathbf{E}} \rangle_{\mathbb{R}^{nd^*} \times \mathbb{R}^{nd}}.$$

where \mathbb{D}^* denotes the adjoint operator for the linear mapping \mathbb{D} . As a consequence of this adjoint transformation, the external kinematic compatible loading $\mathbf{f} \in \mathbb{R}^{nd^*}$ belongs to the same space as the adjoint operator applied to the stress tensor $\mathbb{D}^* \mathbb{A}$. The adjoint operator represents the concept of equilibrium of kinematic compatible forces. The Figure 2.1 presents the equivalence between the internal and external virtual power.

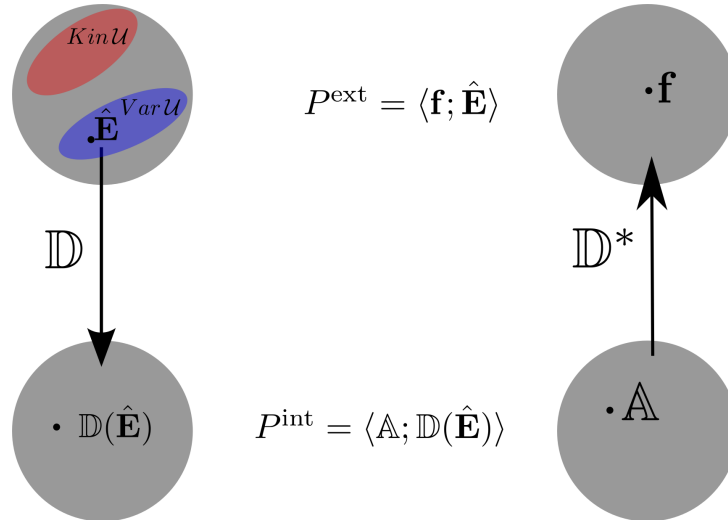


Figure 2.1: Principal elements involved in the PVPB.

2.6 Unconstrained mechanical state manifolds problem

The mechanical state was defined over a manifold that contains restrictions due to the essential boundary conditions and distributed constraints. As shown by [5, 6, 54], it is possible to remove from the adopted manifold (2.3) restrictions like: essential boundary conditions and/or distributed constraints. In these analysis, the distributed boundary constraint, $\mathcal{G}(\mathbf{w}) = 0 \in \Omega$ is removed from the manifold resulting in:

$$\text{Kin } \mathcal{U}_\lambda = \{\mathbf{w} \in \mathbf{H}^1(\Omega) : \mathbf{w}|_{\partial\Omega_D} = \mathbf{E}_D\}. \quad (2.6)$$

Accounting admissible mechanical state's variations, the following subspace is defined:

$$\text{Var } \mathcal{U}_\lambda = \{\mathbf{u}_1 - \mathbf{u}_2 \in \text{Var } \mathcal{U}_\lambda : \mathbf{u}_1, \mathbf{u}_2 \in \text{Kin } \mathcal{U}_\lambda\}. \quad (2.7)$$

The physical problems remains invariant, but the kinematics addressed changes. In order to model the same problem with different kinematic settings, the expression of the PVPB must be updated. In this context, a new kinematic compatible loading λ is introduced over a particular functional space Λ . The functional space Λ has enough regularity to maintain the problem well-posed. In this case λ plays the role of a Lagrange's multiplier, see [9, 15, 51] for more details. The changes in the PVPB yields the following problem:

Problem 2.1 (Unconstrained mechanical state manifolds problem). *Given a source loading function $\mathbf{f} \in \mathbb{R}^{nd^*}$, find the pair $(\mathbf{E}, \lambda) \in \text{Kin } \mathcal{U}_\lambda \times \Lambda$, such that for all $(\hat{\mathbf{E}}, \hat{\lambda}) \in \text{Var } \mathcal{U}_\lambda \times \Lambda$*

$$\begin{aligned} P^{\text{int}}(\mathbb{D}(\hat{\mathbf{E}})) + P^{\text{ext}}(\hat{\mathbf{E}}) &= \langle \mathbb{A}; \mathbb{D}(\hat{\mathbf{E}}) \rangle_{\mathbb{R}^{nd^*} \times \mathbb{R}^{nd}} + \langle \mathbf{f}; \hat{\mathbf{E}} \rangle_{\mathbb{R}^{nd^*} \times \mathbb{R}^{nd}} \\ &+ (\lambda; \mathcal{G}(\hat{\mathbf{E}})) + (\hat{\lambda}; \mathcal{G}(\mathbf{E})) = 0. \end{aligned} \quad (2.8)$$

Once again the adjoint transformation of the linear maps \mathbb{D} and \mathcal{G} are useful for characterizing the functional dependencies between the kinematic compatible loadings $(\mathbb{A} \in \mathbb{R}^{nd^*}, \mathbf{f} \in \mathbb{R}^{nd^*}, \lambda \in \Lambda)$ and the mechanical state variables $(\mathbf{E}, \mathbb{D}(\mathbf{E}))$.

The use of Lagrange multipliers grants the imposition of boundary constraints or distributed restrictions allowing to build up more flexible kinematic admissible manifolds.

In fluid mechanics for example, the use of Lagrange multipliers allows to remove the free divergence restriction from the kinematic admissible manifold to simulate incompressible flows.

2.7 Fluid Mechanics Variational Framework

In this section, based on the three steps modeling procedure, the incompressible Navier-Stokes equations are obtained. The mechanical state is defined in terms of the velocity vector field and the strain rate tensor field, consistently with the first gradient theory, where two different measures of expended power are recognized: internal and external. Thus, the characterization of kinematic compatible loadings is done with the postulation of the PVPB, where the free divergence constraint and fluid-solid interface restriction are weakly enforced by Lagrange multipliers.

2.7.1 Fluid mechanics mechanical state

To start the development some definitions are introduced. The velocity vector field is given by:

$$\begin{aligned} \mathbf{u} : \Omega \times [0, T] &\rightarrow \mathbb{R}^{nd}, \\ (\mathbf{x}, t) &\mapsto \mathbf{u}, \end{aligned} \tag{2.9}$$

where \mathbf{x} represents any arbitrary point of the domain $\Omega \in \mathbb{R}^{nd}$ and t represents an arbitrary time instant of the temporal interval $[0, T]$. The strain rate tensor is introduced as:

$$\begin{aligned} \mathbb{D} &: \text{Lin}(\mathbb{R}^{nd}, \mathbb{R}^{nd}), \\ \mathbf{u} &\mapsto \mathbb{D}(\mathbf{u}) = \nabla \mathbf{u}. \end{aligned} \tag{2.10}$$

Finally for this problem the mechanical state is well-posed by defining the manifold where the velocity vector field lies on:

$$\text{Kin } \mathcal{U} = \{\mathbf{w} \in \mathbf{H}^1(\Omega), \text{essential boundary conditions}\}.$$

The kinematic admissible variations of the mechanical state reside on the following vectorial subspace:

$$\text{Var } \mathcal{U} = \{ \mathbf{u}_1 - \mathbf{u}_2 \in \text{Var } \mathcal{U} : \mathbf{u}_1, \mathbf{u}_2 \in \text{Kin } \mathcal{U} \}.$$

2.7.2 *Fluid mechanics measures of expended power*

The fluid mechanics mechanical state description concluded with the definition of admissible kinematics written in terms of a velocity vector field and a strain rate tensor. As a consequence of this description two measures of expended power can be defined. In one hand the internal power can be written as:

$$P^{\text{int}}(\mathbb{D}(\mathbf{u})) = \langle \mathbb{T}_f; \nabla \mathbf{u} \rangle_{\mathbb{R}^{nd*} \times \mathbb{R}^{nd}};$$

The new element $\mathbb{T}_f \in \text{Lin}(\mathbb{R}^{nd}, \mathbb{R}^{nd})$ is called stress tensor. On the other hand, the external power can be written as:

$$P^{\text{ext}}(\mathbf{u}) = \langle (\mathbf{f} + \rho \mathbf{u} \cdot \nabla \mathbf{u} + \rho \dot{\mathbf{u}}); \mathbf{u} \rangle_{\mathbb{R}^{nd*} \times \mathbb{R}^{nd}},$$

where $\mathbf{f} \in \mathbb{R}^{nd*}$ represents a kinematic compatible external load, $\rho \mathbf{u} \cdot \nabla \mathbf{u} \in \mathbb{R}^{nd*}$ represents the effects of convective forces and $\rho \dot{\mathbf{u}} \in \mathbb{R}^{nd*}$ represents the inertial kinematic compatible loads.

2.7.3 *Fluid mechanics Virtual Power Balance*

Here, the free divergence and the fluid-solid interface constraints are weakly imposed by a Lagrange multiplier. The Lagrange multiplier associated to the divergence free presents the physical behavior of the hydrostatic pressure $p \in L^2(\Omega)$ and the effects of the fluid-solid interface are taken into account considering a Lagrange multiplier $\gamma \in \mathbf{L}^2(\Gamma)$ that enforces the boundary constraint $\mathbf{u} - \mathbf{u}_{sl} = \mathbf{0}$ on Γ .

Problem 2.2 (Incompressible Navier-Stokes equations in presence of a regular obstacle).
Given a source loading function $\mathbf{f} \in \mathbb{R}^{nd*}$, for each $t \in [0, T]$ find the triple $(\mathbf{u}, p, \gamma) \in$

$\text{Kin } \mathcal{U} \times L^2(\Omega) \times \mathbf{L}^2(\Gamma)$, such that for all $(\hat{\mathbf{u}}, \hat{p}, \hat{\boldsymbol{\gamma}}) \in \text{Var } \mathcal{U} \times L^2(\Omega) \times \mathbf{L}^2(\Gamma)$ it satisfies:

$$\begin{aligned} P^{\text{int}} + P^{\text{ext}} &= \int_{\Omega} (\mathbb{T}_f; \nabla \hat{\mathbf{u}}) + (\mathbf{f} + \rho \mathbf{u} \cdot \nabla \mathbf{u} + \rho \dot{\mathbf{u}}; \hat{\mathbf{u}}) - \hat{p} \text{div} \mathbf{u} - p \text{div} \hat{\mathbf{u}} \, d\Omega \\ &+ \int_{\Gamma} (\boldsymbol{\gamma}; \hat{\mathbf{u}}) + (\hat{\boldsymbol{\gamma}}; \mathbf{u} - \mathbf{u}_{sl}) \, d\Gamma = 0, \end{aligned} \quad (2.11)$$

where \mathbf{u}_{sl} is the velocity of the fluid in the solid-fluid interface.

Considering duality arguments [5, 42, 54], the Lagrange multiplier $\boldsymbol{\gamma}$, that enforces the fluid-solid boundary constraints, is identified as a force-like term. Within this context the fluid-solid kinematics can undergo motions concerning translations and rotations, for applications see [18, 25, 27, 53]. For instance, to handle rotations the following expression could be used:

$$\mathbf{u}_{sl} = \begin{bmatrix} 0.0 & \alpha \\ -\alpha & 0.0 \end{bmatrix} \begin{bmatrix} R_x \\ R_y \end{bmatrix},$$

where α is the angular velocity of the obstacle and R_x and R_y denote *radial measures*.

Up to this stage it was possible to recognize the kinematic compatible loadings \mathbf{f} , $\rho \dot{\mathbf{u}}$ and $\rho \mathbf{u} \cdot \nabla \mathbf{u}$, $\boldsymbol{\gamma}$ as terms that are in the dual space \mathbb{R}^{nd*} . In effect they are force-like members and to unveil their relation to the mechanical state the Euler-Lagrange equations are used. In order to obtain the Euler-Lagrange equations associated to the variational problem (2.11) the following adjoint transformations (see [42, 54]) are employed:

$$\int_{\Omega} (\mathbb{T}_f; \nabla \hat{\mathbf{u}}) \, d\Omega = - \int_{\Omega} (\text{div} \mathbb{T}_f; \hat{\mathbf{u}}) \, d\Omega + \int_{\partial\Omega} (\mathbb{T}_f \mathbf{n}; \hat{\mathbf{u}}) \, d\partial\Omega, \quad (2.12)$$

$$\int_{\Omega} p \text{div} \hat{\mathbf{u}} \, d\Omega = \int_{\Omega} (\nabla p; \hat{\mathbf{u}}) \, d\Omega - \int_{\partial\Omega} (p \mathbb{I} \mathbf{n}; \hat{\mathbf{u}}) \, d\partial\Omega, \quad (2.13)$$

where \mathbf{n} denotes the outward unit normal vector to $\partial\Omega$ and \mathbb{I} represents the second order identity tensor. Thus, from (2.11) using the identities (2.12) and (2.13), we derive the following Euler-Lagrange equations that govern the incompressible fluid flow with rigid

obstacles:

$$\left\{ \begin{array}{ll} \rho \dot{\mathbf{u}} + \rho \mathbf{u} \cdot \nabla \mathbf{u} - \operatorname{div} \mathbb{T}_f + \mathbf{f} + \nabla p = \mathbf{0}, & \text{in } \Omega, \\ \operatorname{div} \mathbf{u} = 0, & \text{in } \Omega, \\ (\mathbb{T}_f - p \mathbb{I}) \mathbf{n} = \mathbf{0}, & \text{on } \partial\Omega_N, \\ (\mathbb{T}_f - p \mathbb{I}) \mathbf{n} = \boldsymbol{\gamma}, & \text{on } \Gamma, \\ \mathbf{u} - \mathbf{u}_{sl} = \mathbf{0}, & \text{on } \Gamma, \\ \text{Essential boundary conditions for: } & \mathbf{u}. \end{array} \right. \quad (2.14)$$

The system (2.14) characterizes the force-*like* members \mathbf{f} , $\rho \dot{\mathbf{u}}$, $\rho \mathbf{u} \cdot \nabla \mathbf{u}$ and ∇p as body forces. Furthermore, the Lagrange multiplier that enforces the fluid-solid boundary constraint $\boldsymbol{\gamma}$ shares the same properties as a surface traction vector. It is also possible to note the homogeneous Neumann's boundary conditions, the Dirichlet boundary conditions, the free divergence constraint and the fluid-solid interface constraint. To give closure to the previous problem, the characterization of the internal kinematic compatible loading \mathbb{T}_f is presented. In this case isotropic and Newtonian behavior is assumed yielding the following expression:

$$\mathbb{T}_f = \mu \nabla \mathbf{u},$$

where μ represents the viscosity of the fluid.

The Euler-Lagrange equations (2.14) allows to model the incompressible Navier-Stokes equations considering the inclusion of obstacles to alter the flow. In the next chapter these equations will be discretized by the Lattice Boltzmann Method and, in order to tackle the presence of arbitrary shaped obstacles, two different techniques will be used: the Forcing Method and the Immersed Boundary Method. While the Lattice Boltzmann Method is a technique capable of solving incompressible flows, the inclusion of arbitrary shaped obstacles will be treated "efficiently" employing the Immersed Boundary Method.

3 NUMERICAL METHODS

In this chapter the numerical methods for solving the incompressible Navier-Stokes equations (2.14) and the numerical techniques for dealing with fluid flow around rigid obstacles are presented.

3.1 Introduction

The numerical methods used for solving fluid flow problems are part of a branch of computational mechanics usually called as Computational Fluid Dynamics (CFD). In this context, the Lattice Boltzmann method arises as an alternative to traditional solvers based on the Finite Volume Method (FVM) or Finite Element Method (FEM) that considers a discretized version of the Navier-Stokes equations as the starting point. The LBM describes the kinetics of distribution of particles at the mesoscale. Formally, it can be derived from the Lattice-gas cellular automata's or from a specific discretization scheme of the Boltzmann equation. In the last years the LBM has been successfully applied to study the fluid flow in different applications such as in biomedical engineering [22], heat transfer problems with phase change [60] and also turbulent flows [19].

Traditional numerical methods, such as the FEM, when employed to approximate the Navier-Stokes equations are often challenged by the convective non-linear term, which requires a methodology to linearize the system of equations. Moreover, the problem is commonly approximated in the mixed form, which demands additional computational operations. Other numerical challenge is ensure the free divergence for this problem. In this context, the LBM overcome all these difficulties, because this method naturally treat the non-linear term and does not need to solve the mixed problem to enforce the incompressibility [40, 29] due to the explicit nature of the method, moreover is simple to implement and due to its high locality an efficient parallel implementation can be exploited [10].

To simulate the fluid flow including rigid obstacles using the Lattice Boltzmann Method we employ the Forcing Method [26] and the Immersed Boundary Method [40, 46, 29] to represent the boundary domain conditions and fluid/obstacle interface conditions.

3.2 Lattice Boltzmann Method (LBM)

Here the classical Lattice Boltzmann method for fluid flow is described considering an incompressible fluid. The appropriate treatment of boundary conditions and obstacles are considered within the traditional LBM scheme.

3.2.1 Boltzmann's Equation

Based on the kinetic theory of gases it is possible to show that any changes in the state of pressure, temperature and volume are consequences to the lack of equilibrium between the molecules that interact in the gas. Every molecule in the gas interact with other particles continuously colliding achieving a random motion. As reported in [57] for describing this theory the following assumptions are taken into account:

- the density of a group of molecules might change due to random collisions between other particles; and
- the density of a group of molecules might change due to volumetric forces.

Given a set of particles, in a fixed time t , the particles inside the spatial range $\mathbf{r} + \delta\mathbf{r}$ whose velocity rank is bounded by $\mathbf{c} + \delta\mathbf{c}$ can be measured with the probability distribution function $f(\mathbf{r}, t)$. Neglecting external forces, the kinetic theory of gases establishes the following conservation law known as the *Boltzmann's equation*:

$$\frac{\partial f}{\partial t} + \nabla f \cdot \mathbf{c} = \mathcal{Q}(f); \quad (3.1)$$

where $\mathcal{Q}(f)$ is the *collision operator*, which measures the deviation from equilibrium of the particles. In one hand if $\mathcal{Q}(f) = 0$ the molecules have achieved equilibrium, whereas on the other hand if $\mathcal{Q}(f) \neq 0$ it means that the particles have not achieved a state of equilibrium.

The collision operator defined by Bhatnagar–Gross–Krook (BGK) [7], yields the following expression:

$$\mathcal{Q}(f) = \omega (f^{eq} - f(\mathbf{r}, \mathbf{c}, t)); \quad (3.2)$$

where ω represents the frequency of collisions between the particles and $f^{eq}(\mathbf{r}, \mathbf{c}, t)$ is the so called equilibrium probability distribution. Equations (3.1) and (3.2) when combined

results in the *Boltzmann's equation* with the *BGK-operator*, which is given by

$$\frac{\partial f}{\partial t} + \nabla f \cdot \mathbf{c} = \omega (f^{eq} - f). \quad (3.3)$$

The previous expression forms the basis for the Lattice Boltzmann Method that will be described shortly next. The LBM with the BGK collision operator can be shown to recover the macroscopic behavior of the incompressible Navier-Stokes equations for fluid flow, as shown in [11].

3.2.2 LBM

In order to obtain the expression of the LBM to perform numerical simulations the Boltzmann equation with the BGK-operator (see equation (3.3)) is spanned considering $i = 0, \dots, l$ directions. In this work the spanned directions corresponds to the scheme proposed by He and Luo [24] and also discussed in Mohamad [40]. As a consequence, the following expression is written as:

$$\frac{\partial f_i}{\partial t} + \nabla f_i \cdot \mathbf{c}_i = \omega (f_i^{eq} - f_i). \quad (3.4)$$

In this case the regularity of the interest field f_i grants the possibility to replace the continuous operators (time derivative and spatial gradient) with finite difference schemes for time and space;

$$\frac{\partial f_i}{\partial t} \simeq \frac{f_i(\mathbf{r}, t + \delta t) - f_i(\mathbf{r}, t)}{\delta t}, \quad (3.5)$$

$$\nabla f_i \cdot \mathbf{c}_i \simeq \frac{f_i(\mathbf{r} + \delta \mathbf{r}_i, t + \delta t) - f_i(\mathbf{r}, t + \delta t)}{\|\delta \mathbf{r}_i\|} \frac{\delta \mathbf{r}_i}{\|\delta \mathbf{r}_i\|} \cdot \mathbf{c}_i, \quad (3.6)$$

where $\|\delta \mathbf{r}_i\| = (\delta \mathbf{r}_i; \delta \mathbf{r}_i)^{1/2}$. Replacing (3.5) and (3.6) in the Boltzmann's equation (3.4) we obtain the next equivalence:

$$\frac{f_i(\mathbf{r}, t + \delta t) - f_i(\mathbf{r}, t)}{\delta t} + \frac{f_i(\mathbf{r} + \delta \mathbf{r}_i, t + \delta t) - f_i(\mathbf{r}, t + \delta t)}{\|\delta \mathbf{r}_i\|} \frac{\delta \mathbf{r}_i}{\|\delta \mathbf{r}_i\|} \cdot \mathbf{c}_i = \omega (f_i^{eq} - f_i). \quad (3.7)$$

Considering $\mathbf{c}_i = \delta \mathbf{r}_i / \delta t$ the previous expressions results in the LBM

$$\begin{aligned} \frac{f_i(\mathbf{r} + \delta \mathbf{r}_i, t + \delta t) - f_i(\mathbf{r}, t)}{\delta t} &= \omega (f_i^{eq} - f_i), \\ \rightarrow f_i(\mathbf{r} + \delta \mathbf{r}_i, t + \delta t) &= f_i(\mathbf{r}, t) + \delta t \omega (f_i^{eq} - f_i). \end{aligned} \quad (3.8)$$

The product $\delta t \omega$ defines a new variable τ^{-1} which is known as relaxation parameter. Bearing on numerical methods equation (3.8) is linear, explicit and has great deal of local operations, which allows to perform rapid computations. The relaxation parameter must satisfy the following relation:

$$\mu = \frac{(\delta \mathbf{r}; \delta \mathbf{r})}{3 \delta t} (\tau - 0.5), \quad (3.9)$$

where τ must be greater than 0.5 in order to avoid a fluid with negative viscosity. Lower values of τ represents fluids with a viscosity μ near zero. These fluids will achieve the equilibrium state faster than more viscous fluids.

3.2.3 *Equilibrium Distribution*

The equilibrium distribution characterizes the steady state of the probability distribution function $f(\mathbf{r}, t)$. For particles moving in a macroscopic framework with velocity \mathbf{u} , the *normalized Maxwell-Boltzmann distribution* can be written as follows:

$$f_{MB} = \frac{3 \rho}{2 \pi} \exp \left[-\frac{3}{2} (\mathbf{c} - \mathbf{u})^2 \right], \quad (3.10)$$

where ρ represents the macroscopic density of the fluid. To complete the problem of computing the equation (3.8), the equilibrium distribution is defined when applying a second order asymptotic expansion of the Maxwell-Boltzmann distribution, which yields the following expression:

$$f^{eq} = \phi(\rho) \left(A + B (\mathbf{c}; \mathbf{u}) + C (\mathbf{u}; \mathbf{u}) + D (\mathbf{c}; \mathbf{u})^2 \right), \quad (3.11)$$

where $\{A, B, C, D\} \in \mathbb{R}$ and $\phi(\rho) : \mathbb{R} \rightarrow \mathbb{R}$ that will be defined next.

3.2.4 The D2Q9 Lattice array

In this work, we adopt a *D2Q9* Lattice array (two dimension with nine velocity directions) proposed by He and Luo [24] to perform all simulations. In this context, we can evaluate the *A, B, C* and *D* coefficients where the equations (3.8) and (3.11) are restrict to this scheme. Thus, in a Cartesian frame of reference the *D2Q9* model is given by:

$$\begin{cases} \mathbf{c}_0 = (0, 0), \\ \mathbf{c}_1 = (1, 0) \quad \mathbf{c}_2 = (0, 1) \quad \mathbf{c}_3 = (-1, 0) \quad \mathbf{c}_4 = (0, -1), \\ \mathbf{c}_5 = (1, 1) \quad \mathbf{c}_6 = (-1, 1) \quad \mathbf{c}_7 = (-1, -1) \quad \mathbf{c}_8 = (1, -1). \end{cases} \quad (3.12)$$

These velocity directions are described in Figure 3.1.

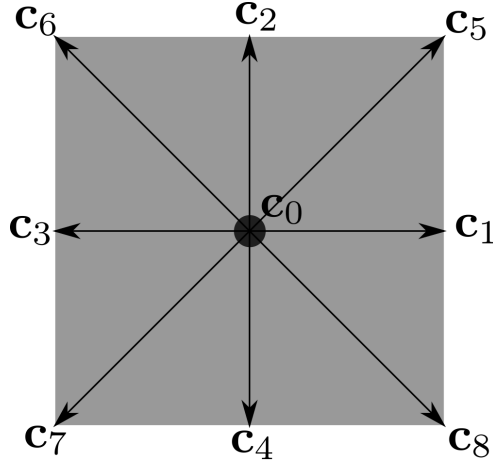


Figure 3.1: The D2Q9 Lattice array.

In the D2Q9 Lattice model it is possible to find particles: at rest (f_0), moving in horizontal and vertical directions ($f_1 - f_4$), and moving in diagonal directions ($f_5 - f_8$). The equilibrium distribution when considering the D2Q9 Lattice model is given by the following expression:

$$f_i^{eq}(\mathbf{c}, t) = w_i \left\{ \rho + \rho_0 \left[1 + 3 \frac{(v \mathbf{c}_i; \mathbf{u})}{v^2} - \frac{3}{2} \frac{(\mathbf{u}; \mathbf{u})}{v^2} + \frac{9}{2} \left(\frac{(v \mathbf{c}_i; \mathbf{u})}{v^2} \right)^2 \right] \right\}, \quad (3.13)$$

where $v = \|\delta \mathbf{r}\| (\delta t)^{-1}$ is the Lattice grid velocity and the weighting directions represented

by w_i are shown next

$$\begin{aligned} w_0 &= \frac{4}{9}, \\ w_1 &= w_2 = w_3 = w_4 = \frac{1}{9}, \\ w_5 &= w_6 = w_7 = w_8 = \frac{1}{36}. \end{aligned}$$

It is important to remark that Chen and Doolen [11] showed that the LBM equation (3.8) with the equilibrium distribution (3.13) recovers the macroscopic behavior of the incompressible Navier-Stokes equations. It is also shown that the LBM is a second order accurate scheme in both time and space. In this work, the equilibrium distribution previously described in general terms with the coefficients A, B, C and D was adapted to ensure improved numerical stability. To this end the guidelines proposed in the research works of Golbert *et al.* [22] and Chen and Doolen [11] were employed.

In order to perform numerical simulations employing the LBM the following work-flow is used:

- 1) Initialization: here the probability distribution functions $f_i(\mathbf{r}, t)$ are initialized;
- 2) Collision: the probability distributions are altered accounting the BGK operator, see the right hand side of equation (3.8);
- 3) Streaming: the probability distributions are streamed to the neighboring nodes following the left hand side of equation (3.8).

After the computations of equation (3.8) with the D2Q9 Lattice model, the macroscopic fluid density ρ and the macroscopic *momentum* are evaluated using the following equations:

$$\begin{aligned} \rho &= \sum_{i=0}^8 f_i, \\ \rho \mathbf{u} &= \sum_{i=0}^8 f_i \mathbf{c}_i. \end{aligned}$$

3.2.5 *Boundary Conditions*

The LBM represented by equation (3.8) recovers the macroscopic behavior of the incompressible Navier-Stokes equations. In the context of the LBM, the boundary conditions like no-slip and/or essential boundary conditions must be treated properly.

Several methods for treating boundary conditions within the LBM have been described in [29, 40]. Periodic boundary conditions are used only when the flow solution is periodic; consequently, periodic boundary conditions conserve mass and momentum at all times. In the bounce-back scheme the probability distributions f_i that hit a rigid wall during the propagation are reflected back considering the incoming direction. The bounce-back scheme is usually applied to impose a no-slip boundary condition. The forcing method applies instantaneous impulses the interface nodes to comply the boundary constraint. This scheme was proposed by Mohamad and Kuzmin [39] and will be detailed next in order to be applied for boundary conditions at rigid obstacles. In order to obtain accurate solutions for the flow around rigid obstacles, with low computational cost the Immersed Boundary Method is presented. Two frames of references are presented in one hand the Eulerian Lattice grid where the fluid is solved. And on the other hand, a Lagrangian set of nodes where the fluid-solid interface is defined.

3.3 Fluid-structure interaction

Here the two techniques used to treat fluid-structure interaction with rigid and moving obstacles within the LBM solver are presented: the forcing method and the Immersed Boundary method (IBM).

3.3.1 *The Forcing Method*

The forcing method [38, 39] imposes the boundary constraints over the Lattice nodes that belongs to the interface a finite impulse. The behavior of the Lagrange's multipliers γ according to Goldstein *et al.* [23] and implemented by Iaccarino and Verzicco [26] is given by:

$$\gamma(\mathbf{r}, t) = c(\mathbf{u}_g(\mathbf{r}, t) - \mathbf{u}(\mathbf{r}, t)) + k \int_0^t (\mathbf{u}_g(\mathbf{r}, t) - \mathbf{u}(\mathbf{r}, t)) dt; \quad (3.14)$$

where following [23, 26] the Lagrange multiplier is defined where \mathbf{u}_g denotes the velocity of the nodes whose Lattices corresponds to the fluid-solid interface, in other words $\mathbf{u}_g = \mathbf{u}_{sl}$ in the fluid-solid interface. Here, k represents a linear elastic constitutive function and c a viscous damping constitutive function. The force term $\gamma(\mathbf{r}, t)$ modifies its magnitude

trailing the discrepancies between a known data-set \mathbf{u}_g and a present data-set \mathbf{u} . This technique was applied in the work of [38] for evaluating the drag and lift forces of a flow considering circular obstacles. Specifically, within the LBM this force field is computed as:

$$\boldsymbol{\gamma}(\mathbf{r}, t) = c(\mathbf{u}_g(\mathbf{r}, t) - \mathbf{u}(\mathbf{r}, t)) + k \sum_n (\mathbf{u}_g(\mathbf{r}, t_n) - \mathbf{u}(\mathbf{r}, t_n)) \delta t_n. \quad (3.15)$$

Then finite impulses are applied to the LBM equation in order to impose the proper boundary condition. The forcing term is applied in each Lattice direction i as [39]:

$$S_i = \frac{\delta t}{v} (\mathbf{c}_i; \boldsymbol{\gamma}). \quad (3.16)$$

Thus the forcing term imposes over the corresponding Lattices a finite impulse given by:

$$\begin{aligned} \sum_{i=0}^8 v S_i(\mathbf{r}, t) \mathbf{c}_i &= \sum_{i=0}^8 \delta t (\mathbf{c}_i; \boldsymbol{\gamma}) \mathbf{c}_i \\ &= \sum_{i=0}^8 \delta t (\mathbf{c}_i; \mathbf{c}_i) \boldsymbol{\gamma} = \delta t \boldsymbol{\gamma} \end{aligned} \quad (3.17)$$

and then the LBM equation (3.8) is modified to include this forcing term as:

$$f_i(\mathbf{r} + \mathbf{c}_i \delta t, t + \delta t) = f_i(\mathbf{r}, t) + \frac{1}{\tau} (f_i^{eq} - f_i(\mathbf{r}, t)) + w_i S_i(\mathbf{r}, t), \quad (3.18)$$

Within this context, it is important to note that the kinematic compatible sources $S_i(\mathbf{r}, t)$ do not alter the balance of the mass, that is

$$\sum_{i=0}^8 w_i S_i(\mathbf{r}, t) = 0.$$

In order to impose boundary constraints like no-slip or Dirichlet boundary conditions, the forcing method imprints over a finite set of Eulerian Lattices a kinematic compatible loading given by equation (3.17). The geometric support for this kinematic compatible loadings is shown in the Figure 3.2.

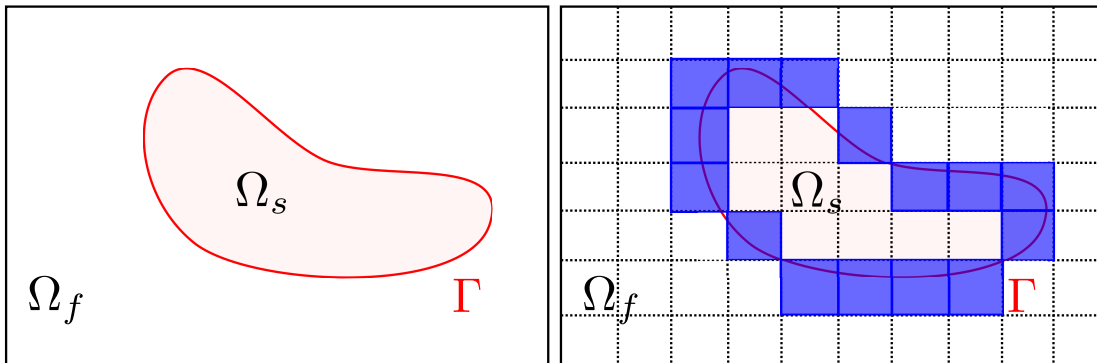


Figure 3.2: Physical situation (left) and forcing method approach (right), the affected Lattices are highlighted in blue.

3.3.2 Immersed Boundary Method

Other alternative to treat the inclusion of arbitrary shaped obstacles is the Immersed Boundary Method. The IBM gives support to the fluid-solid interface considering a Lagrangian set of nodes also known as Lagrangian markers. Hence two frames of references are considered: the flow defined over an Eulerian grid and the fluid-solid interface defined over a finite set of Lagrangian nodes.

When using the classical LBM and the bounce-back scheme or the forcing method of Mohamad [39] for handling boundary conditions around rigid obstacles, some complexity arises since they can have arbitrary and complex geometry, be moving in space or even deformable. If the geometry of the obstacle is complex a staircase approximation such as the one shown in Figure 3.2 would result; if the boundaries are deformable additional constitutive equations have to be considered with the bounce back or a scheme like the forcing method of Mohamad [39], which be very tricky to handle. Therefore, in all these cases the classical LBM is not appropriate and its aforementioned advantages are lost.

Another way of dealing with these challenges is to introduce another mesh composed by Lagrangian nodes that fits the boundary of the solid immersed in the fluid (see Figure 3.3), which is now allowed to deform and move. This way the proper treatment of deformation and movement together with the appropriate constitutive equations is easier. In this direction, one possible method for solving such problems is the Immersed Boundary Method proposed by Peskin [44].

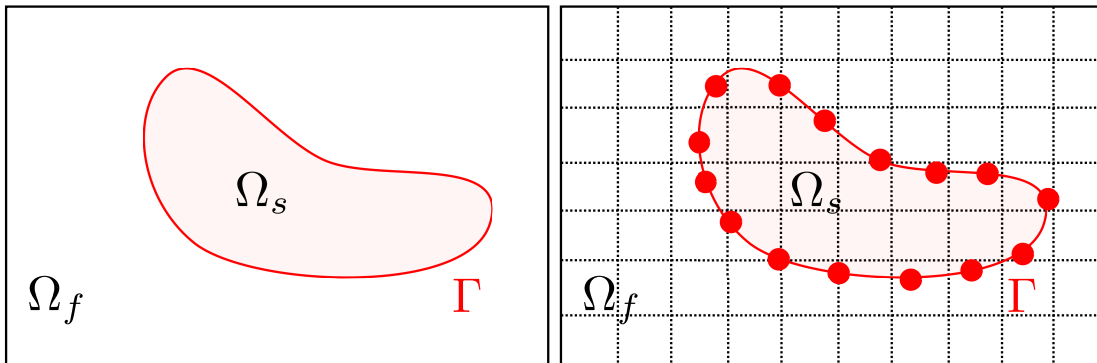


Figure 3.3: Physical situation (left) and IBM approach (right) with Lagrangian nodes highlighted in red.

In FSI analysis the fluid-solid interface might not always agree with the Eulerian fluid description, specially when one considers a complex geometry for the fluid-solid interface. Figure 3.3 shows an example of fluid-solid interface with a complex geometry. A common approach in these cases is to use a very refined grid for representing the complex interface, however it induces a high computational cost. In this context, the IBM Boundary Method arises as a viable option. The IBM represents a modeling technique to include the effects of non-regular interfaces embedded in an Eulerian Lattice grid. In the work of Peskin [46], the IBM uses interpolation schemes for the forces exerted by the solid to the fluid and vice-versa to incorporate the appropriate boundary conditions.

The interpolation scheme for the IBM needs to know the influences of each Lagrangian node towards the Eulerian Lattice grid, and this influences are usually known as *interpolation kernel*. This interpolation kernel associates to every Lagrangian node a finite set of Eulerian Lattices, as shown in Figure 3.4.

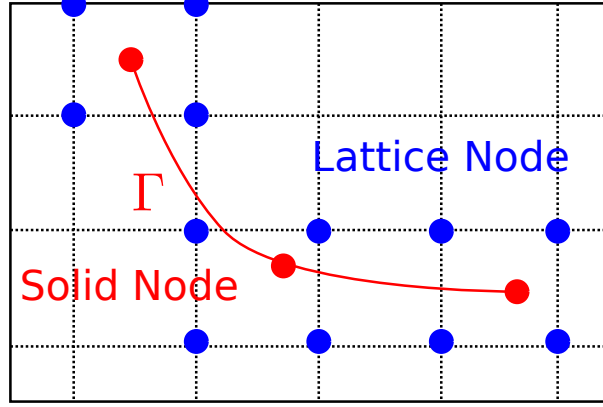


Figure 3.4: IBM interpolation kernel. The interface nodes are colored with red, and the affected Lattice's nodes are highlighted with blue.

Let the coordinates of the Lagrangian nodes be denoted by \mathbf{r} . The main equation for the coupling of LBM and IBM, in a continuous setting, is the equation that describes the no-slip boundary condition:

$$\dot{\mathbf{r}}(t) = \mathbf{u}(\mathbf{r}(t), t), \quad (3.19)$$

where $\dot{\mathbf{r}}(t)$ is the velocity at a Lagrangian node and \mathbf{u} is the LBM velocity. Considering properties of the Dirac's delta function δ , we can rewrite the previous equation as:

$$\dot{\mathbf{r}}(t) = \int_{\Omega} \mathbf{u}(x, t) \delta(\mathbf{x} - \mathbf{r}(t)) d\Omega. \quad (3.20)$$

The other important equation is the one that describes the forces between the solid and fluid, with focus on the forces the solid exerts on the fluid. The following equation describes this relation:

$$\mathbf{F}(\mathbf{x}, t) = \int_{\Gamma} \boldsymbol{\gamma}(\mathbf{r}, t) \delta(\mathbf{x} - \mathbf{r}(t)) d\Gamma,$$

which has to be applied as a volumetric force via the LBM to the fluid.

Considering a computational implementation, the previous expressions have to be discretized with respect to the Dirac delta function. Its discrete version is called here as the interpolation kernel which is represented by the δ_g function ($\delta_g : \Gamma \rightarrow \mathbb{R}$), which gives support for defining the Lagrange multiplier $\boldsymbol{\gamma}$.

The numerically discretized versions of equations (3.19) and (3.20) at each Lagrangian

node $\dot{\mathbf{r}}_k(t)$ are given by

$$\dot{\mathbf{r}}_k(t) = \sum_{\mathbf{x}} \|\delta\mathbf{r}\|^3 \mathbf{u}(\mathbf{x}, t) \delta_g(\mathbf{r}_k, \mathbf{x}) \quad (3.21)$$

$$\mathbf{F}(\mathbf{x}, t) = \sum_k \boldsymbol{\gamma}_k(t) \delta_g(\mathbf{r}_k, \mathbf{x}) \quad (3.22)$$

where $\|\delta\mathbf{r}\|$ denotes a measure of the Eulerian grid, $\boldsymbol{\gamma}_k(t)$ the force at the Lagrangian node k and \mathbf{u} and \mathbf{r}_k represents Eulerian and Lagrangian coordinates, respectively.

Considering that the delta function can be decomposed as $\delta_g(\mathbf{r}_k, \mathbf{x}) = \phi(x)\phi(y)$, then the following ϕ function was employed:

$$\phi(x) = \begin{cases} 1 - |x|, & \text{if } 0 \leq |x| \leq 1, \\ 0, & \text{if } 1 \leq |x|. \end{cases}$$

$$\phi(y) = \begin{cases} 1 - |y|, & \text{if } 0 \leq |y| \leq 1, \\ 0, & \text{if } 1 \leq |y|. \end{cases}$$

For more details on properties and requirements of the discrete Dirac delta functions as well as alternative delta functions see [46]. Moreover, in the works [13, 29, 30, 46] different closed expressions are given for characterizing the δ_g function.

3.3.3 IBM for rigid obstacles

The IBM implementation strategy, as described in the works of [46, 16, 30], assume that the forces that are interpolated from the fluid to the solid and vice-versa are always proportional to changes in the position of the Lagrangian nodes that are,

$$\boldsymbol{\gamma}(\mathbf{r}_k, t) = k \int_0^t (\mathbf{u}_{sl}(\mathbf{r}_k, t) - \mathbf{u}(\mathbf{r}_k, t)) dt, \quad (3.23)$$

where $\mathbf{u}_{sl}(\mathbf{r}_k, t) dt$ denotes a known position of any Lagrangian node, and $\mathbf{u}(\mathbf{r}_k, t) dt$ represents the actual position of the Lagrangian node.

In this work, we adopt a scheme that considers the discrepancies of Lagrangian positions

and Lagrangian velocities as well, and is given by:

$$\gamma(\mathbf{r}_k, t) = c(\mathbf{u}_{sl}(\mathbf{r}_k, t) - \mathbf{u}(\mathbf{r}_k, t)) + k \int_0^t (\mathbf{u}_{sl}(\mathbf{r}_k, t) - \mathbf{u}(\mathbf{r}_k, t)) dt. \quad (3.24)$$

In order to include the previous force member in the LBM, the corresponding forcing term results in:

$$\gamma(\mathbf{r}_k, t) = c(\mathbf{u}_{sl}(\mathbf{r}_k, t) - \mathbf{u}(\mathbf{r}_k, t)) + k \sum_i (\mathbf{u}_{sl}(\mathbf{r}_k, t_i) - \mathbf{u}(\mathbf{r}_k, t_i)) \delta t_i. \quad (3.25)$$

3.3.4 Parameters for fluid-structure interaction simulations

Every simulation involving the IBM and forcing method whose corresponding sources functions are described in equations (3.25) and (3.15) respectively, were executed with the values shown in the Table 3.1.

Table 3.1: IBM coefficients used in this work.

Magnitude	Domain Ω	Boundary $\partial\Omega, \Gamma$
\mathbf{u}	$c = 1.0E - 04$	$c = 7.0E - 05$
	$k = 1.0E - 06$	$k = 7.0E - 08$

To obtain the numerical results shown in this work, the equilibrium distribution proposed by He and Luo [24], written in equation (3.13) was changed to grant numerical stability. Those changes are presented in the Table 3.2.

Table 3.2: Equilibrium distribution optimal coefficients to ensure stability.

Velocity direction	A	B	C	D
\mathbf{c}_0	0.373	0.000	0.400	0.000
$\mathbf{c}_1 - \mathbf{c}_4$	0.147	0.333	-0.200	0.000
$\mathbf{c}_5 - \mathbf{c}_8$	0.010	0.083	-0.025	0.125

The coefficients shown in the previous table are the result of a stability pre-processing. The LBM equation (3.8) allows to compute solutions explicitly, as a consequence the stability is conditioned to a relation between the spatial Lattice grid refining and the temporal discretization. To improve the stability one can:

- adjust the values of the relaxation parameter τ , defined in terms of the viscosity (see equation (3.9));
- or, choose the coefficients of the equilibrium distribution to ensure stability (see equation (3.11)).

According to the works of Golbert *et al.* [22] and Chen and Doolen [11], the stability of the LBM can be measured considering the spectral radius of the second order tensor that represents the equation (3.8) under harmonic perturbations.

In this work the equilibrium distribution was submitted to the constraints shown in the work of Golbert *et al.* [22]. As a consequence of this procedure the relation between the coefficients $\{A, B, C, D\} \in \mathbb{R}$ is established and fixed to ensure numerical stability. All the numerical experiments of this work were carried out considering the parameters shown in Table 3.2.

4 NUMERICAL RESULTS

In this chapter the numerical experiments carried out in this work are presented with focus on validating the LBM solver and the treatment of fluid-solid interface flow problems. Comparisons with data available from the literature and analytical solutions are done in this analysis.

4.1 Kovasznay problem

The *Chapman-Enskog* expansion performed by Chen and Doolen in [11] shows that the equation (3.8) when employing the *D2Q9* Lattice model proposed by He and Luo [24] obtains the solution of the incompressible Navier-Stokes equations with second order convergence rate. To validate the LBM solver and check the second order accuracy the *Kovasznay flow* problem was used. The analytical solution for this problem, described in [28], is given by:

$$u_x = 1 - \exp(\lambda x) \cos(2\pi y), \quad (4.1)$$

$$u_y = \frac{\lambda}{2\pi} \exp(\lambda x) \sin(2\pi y), \quad (4.2)$$

$$p = -\frac{1}{2} \exp(2\lambda x) + C, \quad (4.3)$$

where C is a constant parameter fixed as $C = 0$ and λ is defined as

$$\lambda = \frac{R_E}{2} - \sqrt{\left(\frac{R_E}{2}\right)^2 + (2\pi)^2}. \quad (4.4)$$

The domain $\Omega = (0, 2) \times (-0.5, 1.5)$ was refined with several arrangements as shown in Table 4.1. For validating the implemented CFD solver the forcing method was used, considering $c = 0.0$. The Dirichlet boundary conditions were obtained from the exact solution. In this experiment the Reynolds number was fixed as 20 and the number of iterations of the LBM were fixed as 1000. The flow pattern for this benchmark case is shown in Figure 4.1.

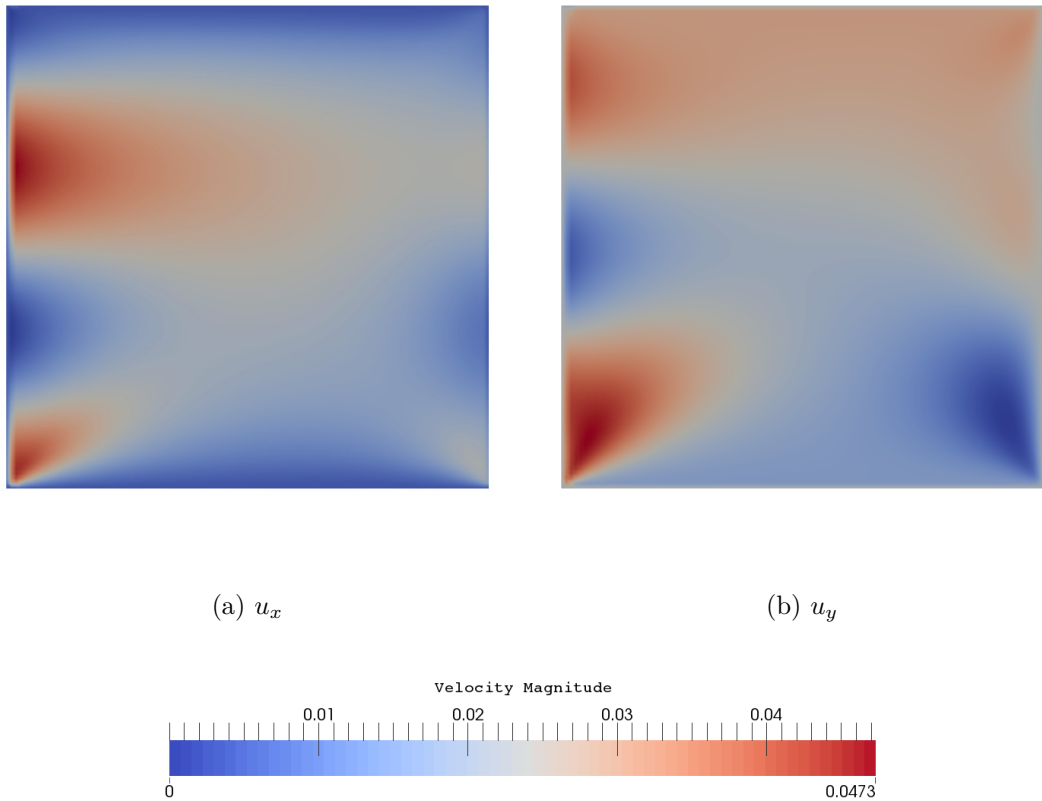


Figure 4.1: Velocity field for the Kovaszny flow.

The spatial convergence of the LBM is shown in Table 4.1. Here it is possible to note that the error decreases with the expected convergence ratio towards grid refining, allowing to validate the CFD solver based on the LBM.

Table 4.1: History convergence for Kovaszny Flow.

Lattice Array	$\ \mathbf{u}_{Exact} - \mathbf{u}_{LBM}\ _{\infty}$	Convergence Order
64×64	$0.22130E - 03$	–
128×128	$0.54903E - 04$	2.01
256×256	$0.13671E - 04$	2.00
512×512	$0.34076E - 05$	2.00
1024×1024	$0.83520E - 06$	2.02

The Kovaszny flow was used to compare the convergence of both IBM schemes. In one hand, the classic IBM scheme described in equation (3.23). And on the other hand, the enhanced IBM scheme described in equation (3.24). The Figure 4.2 compares the error behavior for both schemes considering variations on the k coefficient.

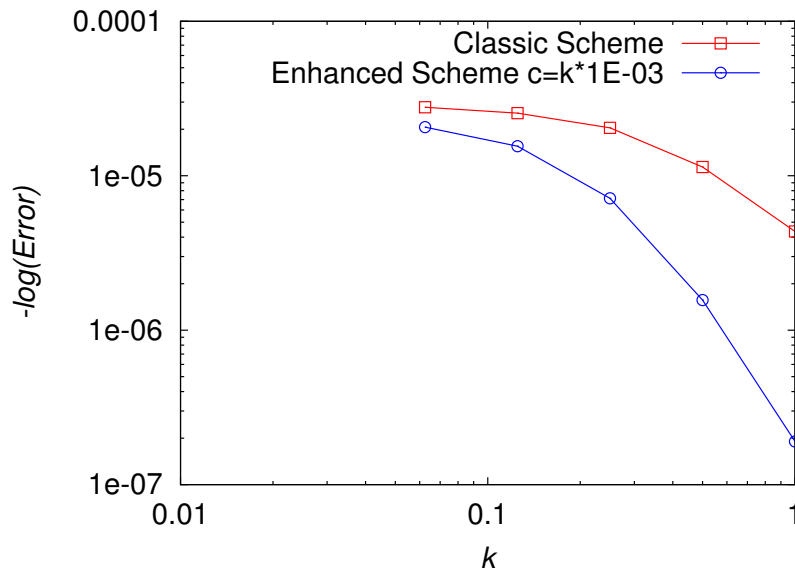


Figure 4.2: Comparison between the classic IBM scheme (3.23) vs. the enhanced IBM scheme (3.24).

In this comparison it is possible to note that the enhanced scheme for evaluating the force-like term results more accurate than the classic scheme. Thus, when referring to the IBM the enhanced method will be addressed.

4.2 Flows with rigid obstacles

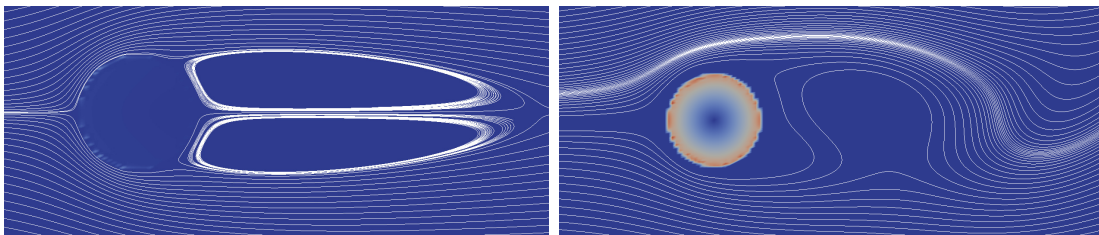
In this section, numerical results are presented to validate the LBM for solving the incompressible Navier-Stokes equations with rigid obstacles. In these studies, well known important flow coefficients such as *drag* and *lift* were studied considering various Reynolds numbers. The obtained values from numerical simulations were compared with exact solutions or data from literature.

4.2.1 Flow around a spinning circle

The following experiment attempts to model the *inverse Magnus effect* employing the forcing method to impose a spin boundary constraint. This phenomenon takes place when the bulk flow is modified due to the presence of a spinning obstacle. The obstacle itself alters the bulk flow, nevertheless if the obstacle spins over its geometrical axis the resultant flow is non-symmetric. This problem has been studied before by [18, 25, 53, 27], showing

a compelling need of computational mechanics to simulate and understand the motion actions like drag and lift forces when the obstacle rotates.

Figure 4.3 shows the streamlines for two different flowing conditions: fixed obstacle and spinning obstacle. Note that due to the use of the forcing method, the obstacle itself is not explicitly shown in the colour maps, except in Figure 4.3 (b) where it is evident due to the spinning velocity.



(a) Without spin motion action

(b) With spin motion action

Figure 4.3: Flow patterns analysis considering $R_E = 20$. The contour maps corresponds to the distribution of the $\gamma(\mathbf{r}, t)$ vector field.

In this context, it is interesting to evaluate the drag and lift forces considering variations of the angular velocity. Then if the Reynolds number turns singular, the Stokes flow equation retrieves analytic expressions, see [25]. In particular the following expressions are given for the drag and lift forces:

$$F_{Drag} = 3\pi\rho d(\alpha + u_x)^2, \quad (4.5)$$

$$F_{Lift} = \frac{\pi}{8}d^3\rho u_x\alpha, \quad (4.6)$$

where α is the angular velocity, u_x is the horizontal velocity value (fixed in $u_x = 0.01$), d is the diameter of the circular obstacle (fixed in $d = 10$).

In this case variations for angular velocities and Reynolds number were done. The Figure 4.4 shows the agreement between the exact solution, given by equation (4.5), and the LBM numerical results for very low Reynolds numbers.

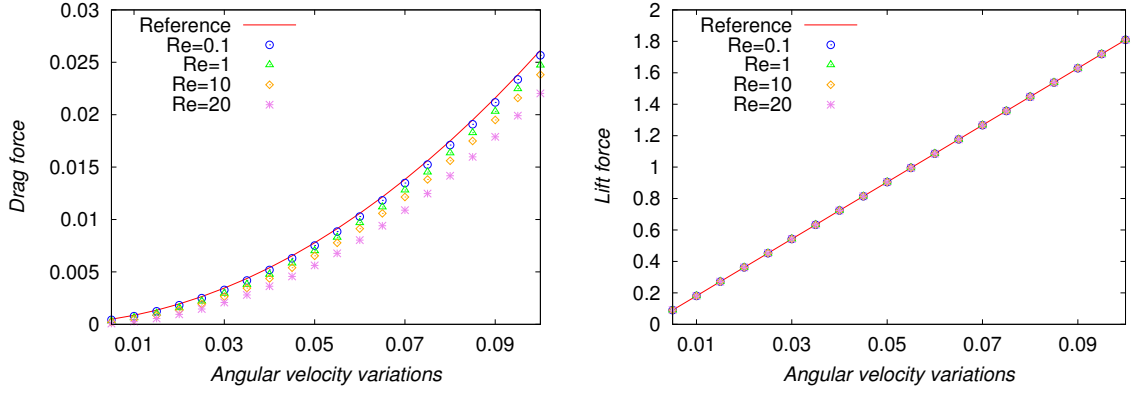


Figure 4.4: Drag and lift forces for different Reynolds numbers.

4.2.2 Turek's Benchmark

The compilation made by Turek and Schafer [59], proposes a broad range of problems for evaluating the performances of numerical CFD solvers. The problems that Turek and Schafer proposes in [59] allow to understand flow around a cylinder and assess the results obtained by different numerical solvers. In this work the first problem of the mentioned benchmark, entitled as *Test case 2D-1 (steady)*, was studied. The geometry and boundary conditions for this case are shown in Figure 4.5.

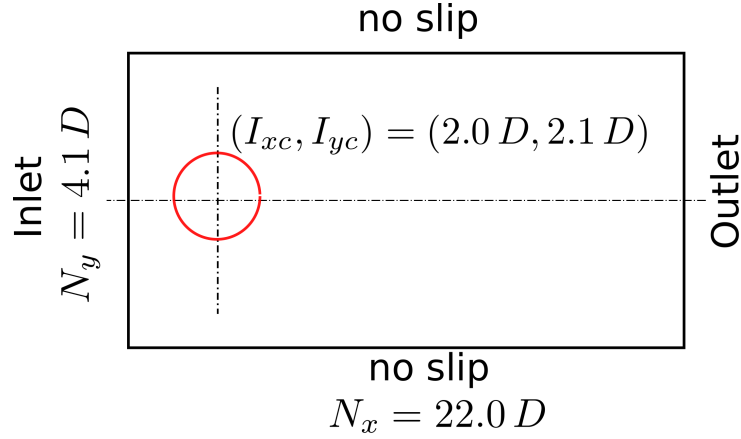


Figure 4.5: Geometry of the flow around a cylinder, the geometry was re-scaled to Lattice units.

For the *Test case 2D-1 (steady)* benchmark case the inflow, satisfies the following expression:

$$u_x = \frac{4 u_{x0}}{N_y^2} y (N_y - y), \quad u_y = 0.0,$$

where $u_{x0} = 0.3$. The Reynolds number was fixed in $R_E = 20.0$. For this analysis the outflow assumed periodic boundary conditions.

Several research groups obtained solutions for the proposed benchmark problem using different CFD methods like solvers based on the Finite Difference Method, the Finite Volume Method, the Finite Element Method and the LBM-BGK. In Figure 4.6 it is possible to see the solutions that several research groups obtained for the benchmark case considering some important parameters of the problem under study.

For this experiment, the implemented CFD solver will be compared using the Degrees of Freedom ($\#DOF$), drag coefficient (C_D) and lift coefficient (C_L), which are highlighted in blue in Figure 4.6 for all the participants of the benchmark.

	Unknowns	c_D	c_L	L_a	ΔP	Mem.	CPU time	MFlop rate
1	200607	5.5567	0.0106	0.0845	0.1172	15	788	1600 PEAK
	51159	5.5567	0.0106	0.0843	0.1172	4	273	
	13299	5.5661	0.0105	0.0835	0.1169	1	144	
3a	10800	5.6000	0.0120	0.0720	0.1180	2.5	121	75 PEAK
4	297472	5.5678	0.0105	0.0847	0.1179	137	31000	445 LINP
	75008	5.5606	0.0107	0.0849	0.1184	73	8000	
	19008	5.5528	0.0118	0.0857	0.1199	57	2000	
6	1314720	5.8190	0.0110	0.0870	0.1230	40	80374	13 LINP
	332640	5.7740	0.0030	0.0830	0.1230	10	10461	
	85140	5.7890	-0.0060	0.0870	0.1230	2.6	1262	
7a	294912	5.5846	0.0106	0.0846	0.1176	75	192	13 LINP
	73728	5.5852	0.0105	0.0845	0.1176	19	47	
	18432	5.5755	0.0102	0.0842	0.1175	5	13	
8a	20487	5.5760	0.0110	0.0848	0.1170	9.0	2574	8.3 LINP
	6297	5.5710	0.0130	0.0846	0.1160	2.9	362	
	2298	5.4450	0.0200	0.0810	0.1110	1.3	109	
9a	240000	5.5803	0.0106	0.0847	0.1175	53	9200	34 LINP
	60000	5.5786	0.0106	0.0847	0.1173	10	1400	
	15000	5.5612	0.0109	0.0848	0.1166	2.5	200	
10	2665728	5.5755	0.0106	0.0780	0.1173	350	677	90 LINP
	667264	5.5718	0.0105	0.0770	0.1169	89	169	
	167232	5.5657	0.0102	0.0730	0.1161	22	52	
	42016	5.5608	0.0091	0.0660	0.1139	5	18	
12	32592	5.5069	0.0132	0.0830	0.1155	18	1796	5.5 LINP
	26970	5.5125	0.0056	0.0827	0.1154	15	1099	
	22212	5.6026	-0.0031	0.0815	0.1167	13	3437	
13a	25410	5.6145	0.0159	0.8315	3.0002	4	14203	90 LINP
	12738	5.6114	0.0169	0.8224	2.9943	2	3018	
	6562	5.7377	0.0514	0.8107	3.2277	1		
14a	3077504	5.6323	0.0137	0.0782	0.1159	214	15300	6.6 LINP
	768704	5.6382	0.0102	0.0775	0.1156	53	5490	
	191840	5.5919	-0.0009	0.0750	0.1143	13	2800	
14b	30775296	5.5902	0.0108	0.0853	0.1174	5340	1534	1334 LINP
	7695104	5.6010	0.0110	0.0844	0.1174	1341	400	
	1922432	5.6227	0.0113	0.0833	0.1172	338	119	
14c	797010	5.5708	0.0167	0.0837	0.1168	460	8000	334 LINP
	363457	5.5598	0.0142	0.0835	0.1166	230	3290	
	176396	5.5106	0.0046	0.0835	0.1150	110	2560	
15a	432960	5.5602	0.0329	0.0730	0.1054	4.4	179986	7.4 LINP
	108240	5.6300	0.0751	0.0720	0.1037	1.1	13593	
	27060	5.7769	0.2085	0.0680	0.0998	0.3	688	
17	111342	5.5610	0.0107		0.1170	87	2568	8.3 LINP
	60804	5.5520	0.0102		0.1168	47	1092	
	19416	5.5160	0.0099		0.1158	15	373	
	lower bound	5.5700	0.0104	0.0842	0.1172			
	upper bound	5.5900	0.0110	0.0852	0.1176			

Figure 4.6: Available solutions handed out for *Test case 2D-1 (steady)*, the solutions highlighted in red corresponds to the research group that employed a LBM-BGK CFD solver. Adapted from [59].

Here the drag and lift forces were measured employing the scheme proposed by Mei *et al* [38], represented with equation (3.17). The simulations are performed by two methodologies to represent the inclusion of obstacles. The forcing method of Mohamad [39] requires a high grid refinement to properly represent the circular cylinder precisely. The IBM combines two different frames of references (Eulerian references for the fluid and Lagrangian references for the fluid-solid interface), and therefore is expected to better represent the circular fluid-solid interface.

Concerning the upper-bounds and lower-bounds shown in Figure 4.6, which are recommended values for the drag and lift coefficients proposed by Turek and Schafer, the research group 6 reported solutions employing a LBM-BGK based CFD solver. The solution obtained by this research group are far away from the solutions obtained with other numerical methods. In this work, both the forcing method and IBM presents solutions for the drag and lift coefficient in closer to the available bounds than the one obtained by group 6 of the Turek’s benchmark. The Figure 4.7 shows a comparison of Forcing method and IBM to describe the drag and lift coefficients when increasing of the number of degrees of freedom (#DOF).

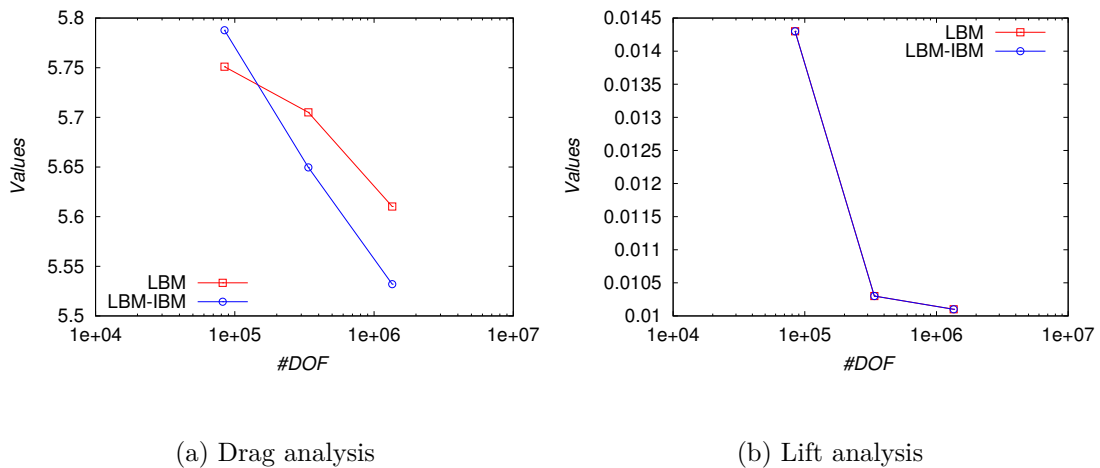


Figure 4.7: Forcing method vs IBM, drag and lift analysis.

Both methods resulted in solutions for the drag and lift coefficients in agreement with the bounds shown in Figure 4.6. In what concerns the computational cost and performance, the IBM results a method that is more efficient than the Forcing method. From now and beyond when modeling flows altered with the presence of obstacles the IBM will be used to simulate the proposed problem.

Figure 4.8 compares the contour maps for the velocity obtained employing the forcing method and the IBM. In this simulations, the forcing method requires 539000 nodes for the LBM to solve the problem and only 339 Lattices were related to the circular inclusion. In the forcing method the grid refinement was done in all the computational domain until the drag coefficient was between the upper and lower bounds, see Figure 4.6. On the other hand the IBM obtained solutions that required 77000 nodes to solve the problem within the same accuracy (between lower and upper bounds of the drag and lift coefficients). In this case, only 52 Lagrangian nodes were used to represent the circular obstacle. In terms of computational performance, the forcing method requires 200 minutes to complete 10000 iterative steps, while the IBM requires only 81 minutes to complete the simulation.

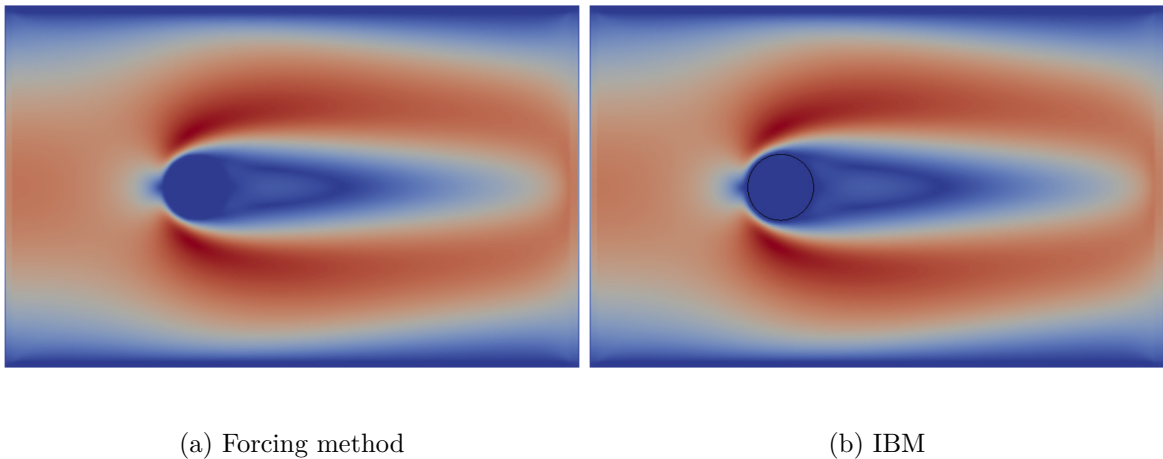


Figure 4.8: Velocity contour maps comparison. (a) forcing method and (b) IBM.

4.2.3 *Flow around a cylinder*

In this experiment the LBM-IBM is used to solve the flow around a circular cylinder subjected to the boundary conditions as described in Figure 4.9. This benchmark problem was proposed in [13, 38] consisting in a circular cylinder immersed in a rectangular channel through where the fluid flows.

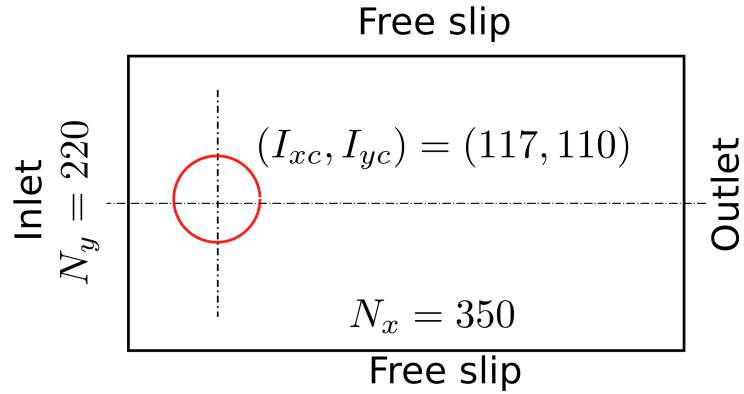


Figure 4.9: Geometry of the flow around a cylinder.

In this case the cylinder diameter has 16.66 units and the inlet flow velocity is given by:

$$u_x = \frac{4u_{x0}}{N_y^2} y(N_y - y), \quad u_y = 0.0,$$

where $u_{x0} = 0.1$ represents the maximum value of u_x .

Figure 4.10 shows the resulting flow considering five different Reynolds numbers, $R_E = \{50, 75, 100, 125, 150\}$. The Lattice grid size was fixed for all the simulations and the simulations were carried out for $1.0E + 05$ iterative steps.

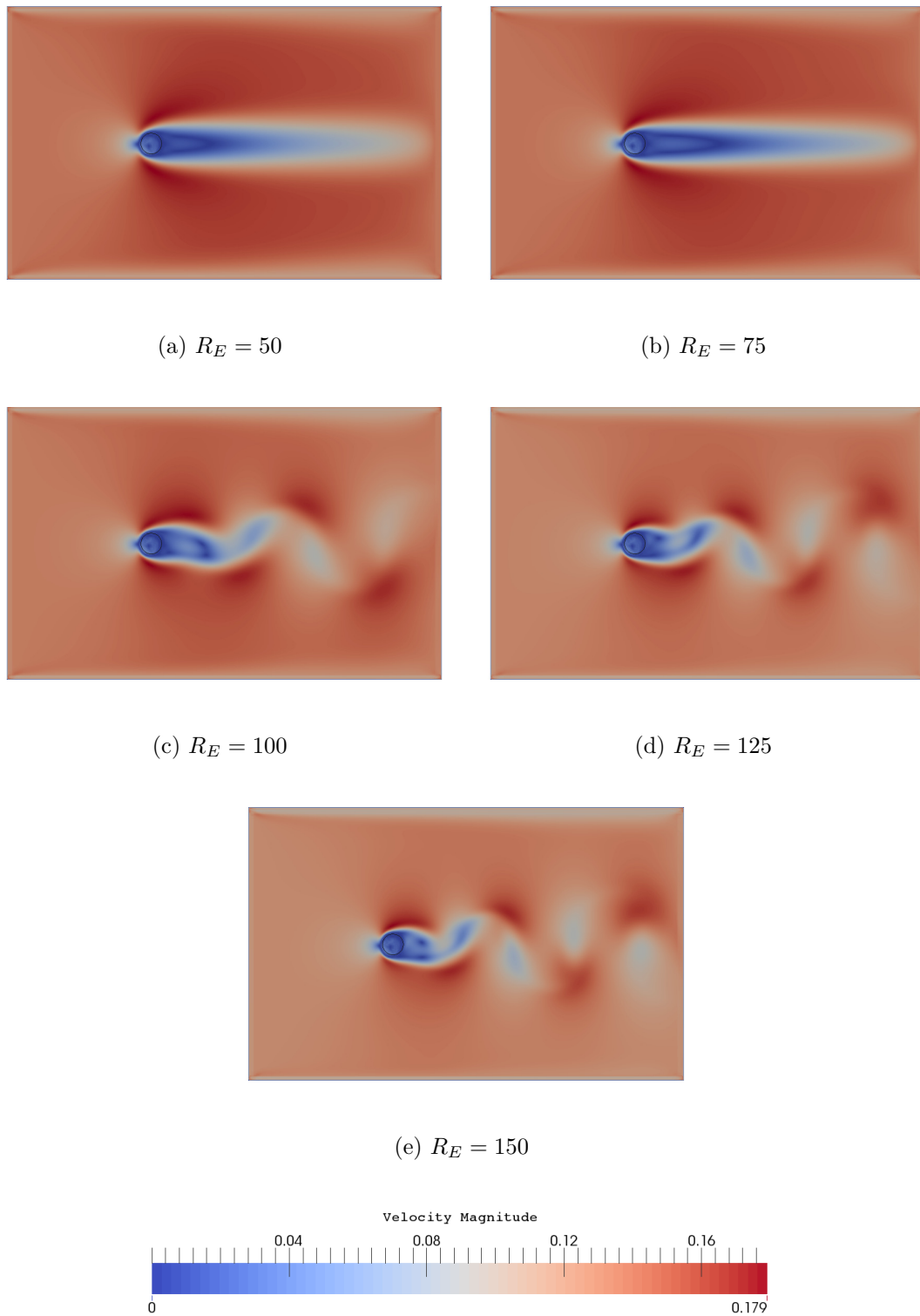


Figure 4.10: Flow around a circular cylinder: Velocity field considering different Reynolds numbers.

The relationship between the drag coefficient and the Reynolds number was analyzed and is shown in Figure 4.11.

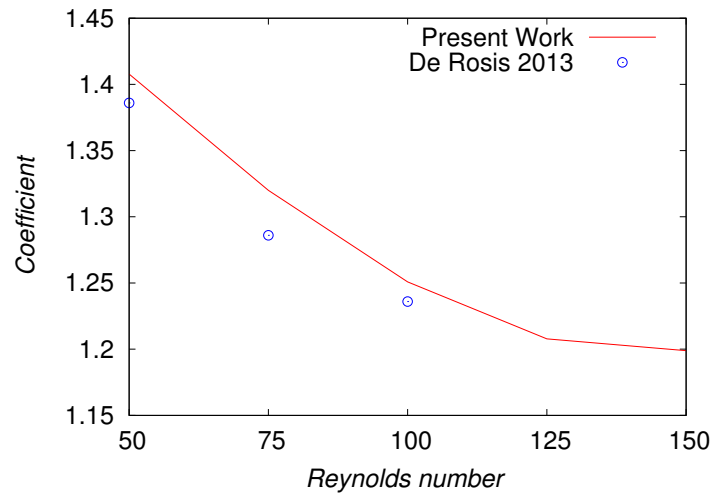


Figure 4.11: Drag coefficients at different Reynolds numbers.

In this case the drag decreases its value till stagnation towards 1.2 for increments of the Reynolds number. The same behavior was observed in [13] allowing to validate the technique for evaluating the drag coefficient (and drag force).

4.2.4 The von Karman Vortex Street

According to [31, 52, 61] the so called *von Karman vortex street* can be used as a benchmark problem to evaluate the stability of the numerical implementation. In this context, the LBM-IBM was employed to study the flow considering a circular cylinder that alters the bulk flow. The domain characteristics and boundary conditions are shown in Figure 4.12, where it is important to note that this case differs from the previous one by the presence of the no-slip condition at the top and bottom of the domain. Both inlet and outlet flow satisfies the same velocity profile as in the previous case.

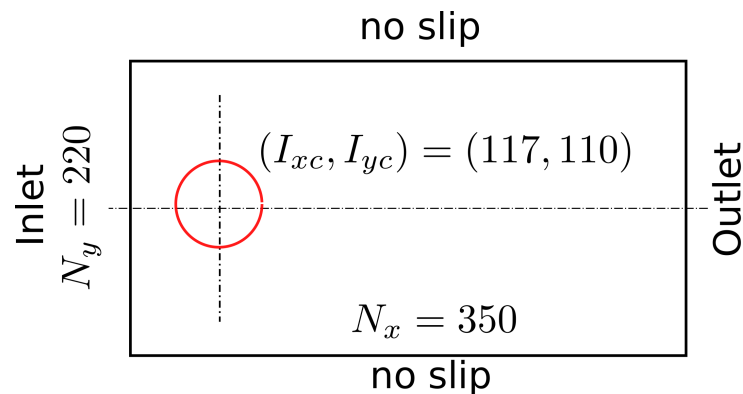
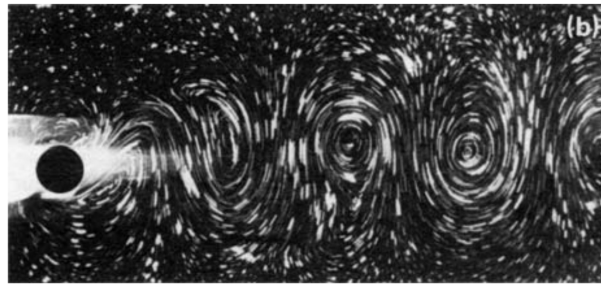
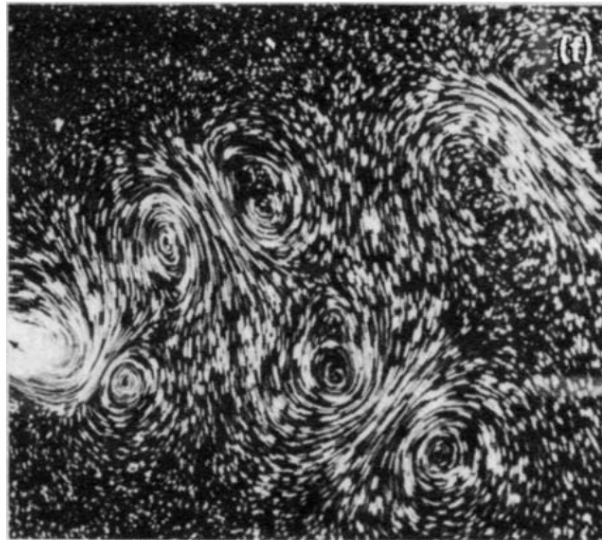


Figure 4.12: Geometry of the flow around a cylinder.

The objective of this experiment is demonstrate that the LBM-IBM is able to capture physical instabilities like the *boundary layer separation*. As reported by [52, 61] the boundary layer separation is materialized with the apparition of a regular array of vortices rotating clockwise and counter-clockwise. In this context the instability imprints transient loads. Regarding structural dynamics it is important to study the frequency of the boundary layer separation to avoid resonance effects in the structure. In this case the Vortex-Induced-Vibrations (VIV) studied in deep by Williamson and Govardhan [61] recognizes two major separation patterns known as "2S and 2P", see Figure 4.13.



(a) 2S mode (2 single vortices)

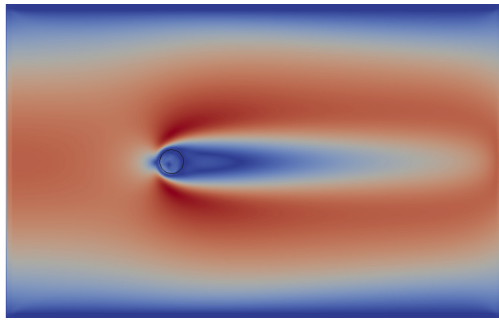


(b) 2P mode (2 pair vortices)

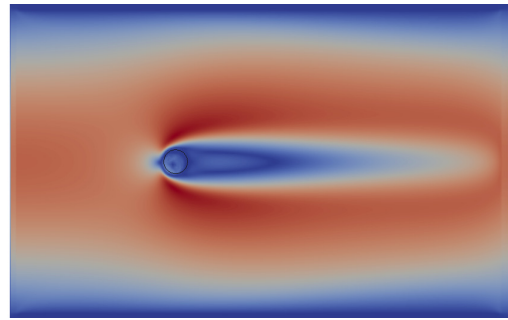
Figure 4.13: Vortex principal separation modes. Adapted from [61].

In this experiment, five different scenarios were considered characterized by the following Reynolds numbers: $R_E = \{50, 75, 100, 125, 150\}$. The Lattice grid is depicted in Figure 4.12. In Figure 4.14 it is possible to observe the contour maps for the velocity field after

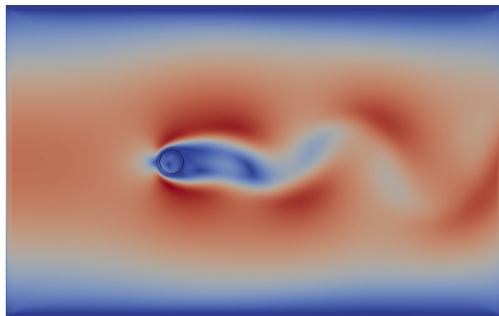
performing $1.0E + 05$ iterative steps.



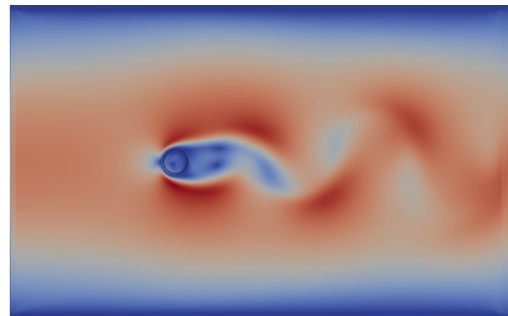
(a) $R_E = 50$



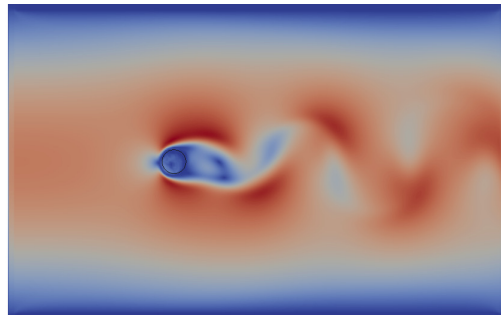
(b) $R_E = 75$



(c) $R_E = 100$



(d) $R_E = 125$



(e) $R_E = 150$

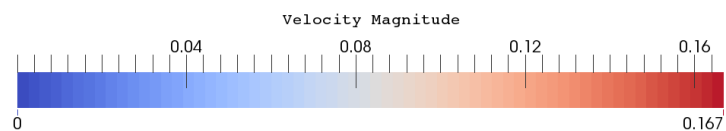


Figure 4.14: Velocity field.

When analyzing the solutions shown in Figure 4.14 it is possible to acknowledge that the simulations with Reynolds number greater or equal to 100 allows to witness the von

Karman vortex street effects. The Reynolds number in these cases can be used as a threshold for analyzing the VIV effects as reported by the works of [31, 52].

Here it is important to characterize the vortex principal separation modes (2S and 2P). To do this the following analysis was done considering three equidistant points with the labels: "A" representing the node with coordinates $(0.25 N_x, 0.5 N_y)$, the label "B" the node with coordinates $(0.5 N_x, 0.5 N_y)$ and the label "C" the node with coordinates $(0.75 N_x, 0.5 N_y)$. These three points allowed to understand effects before the obstacle, near the obstacle and after the obstacle. The Figures 4.15 and 4.16 shows the variations of the velocity vector field, components u_x and u_y , respectively.

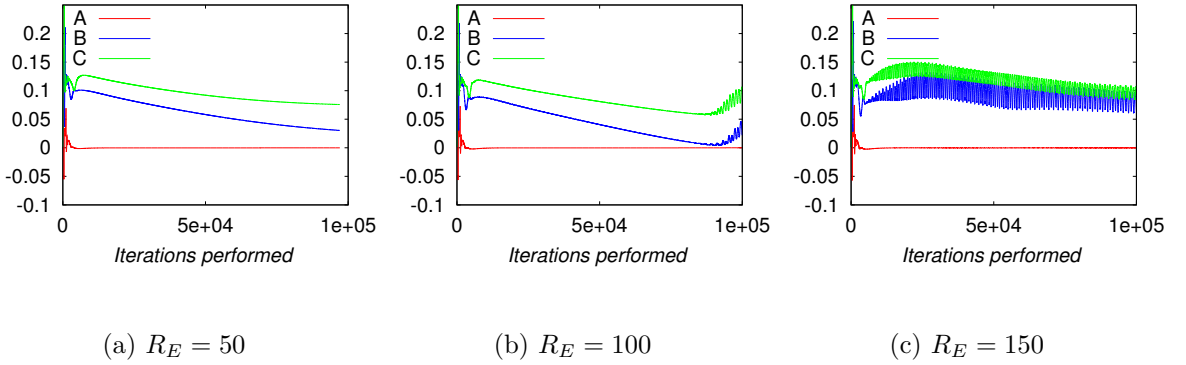


Figure 4.15: u_x field variations during the simulations.

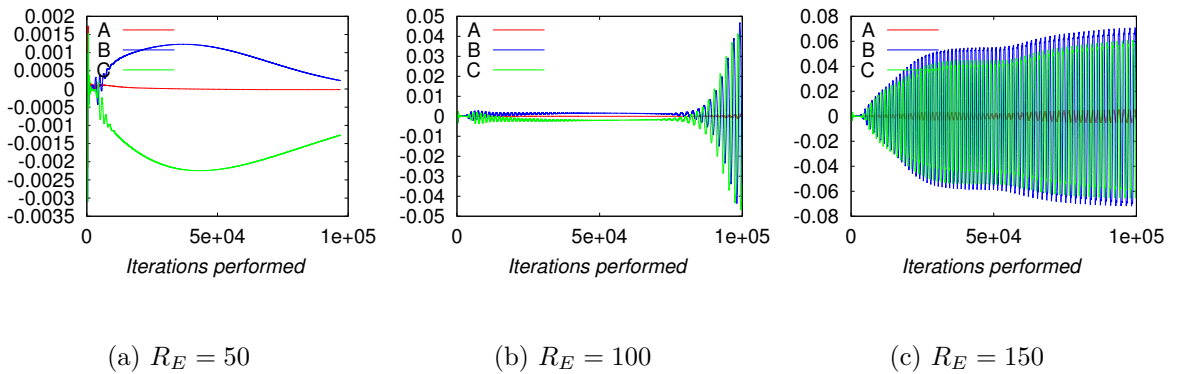


Figure 4.16: u_y field variations during the simulations.

The previous figures allows to distinguish only one frequency of the boundary layer separation, in deed the frequency corresponds to a vortex separation mode 2S. To conclude this experiment in Figure 4.17 the density variations are shown for the same three interest points. The incompressibility constraint was successfully imposed as can be seen from

density, and the consequences are: the flow before the obstacle reduces the density (reducing the pressure) and the flow after the obstacle increases the density (increasing the pressure), in this case the mean value corresponds to the interest point near the obstacle, this value is constant null.

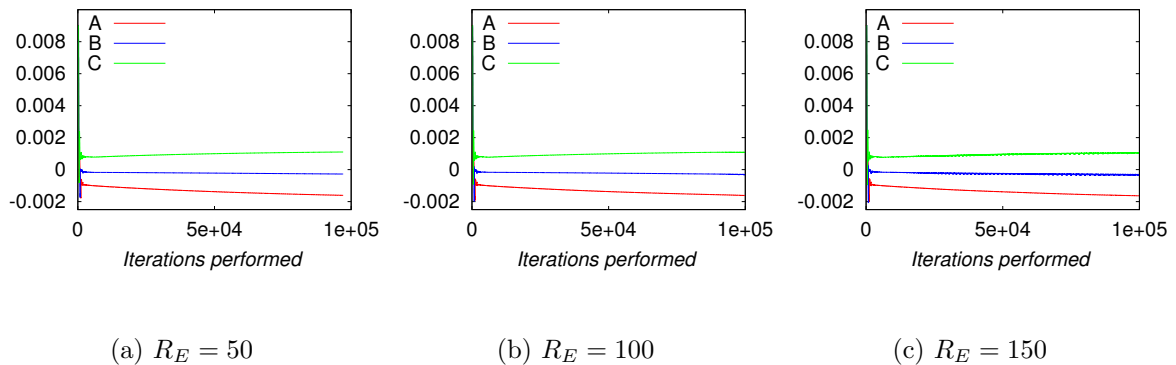


Figure 4.17: Density variations during the simulations.

4.2.5 Flow Around a Square Cylinder

In the next problem, we consider that the flow is altered with the inclusion of a square cylinder. The characteristic length of the square is fixed in $D = 10$. The geometry and boundary conditions are obtained from [8, 13], and depicted in Figure 4.18. For this experiment the velocity inlet profile remains the same as in the previous cases.

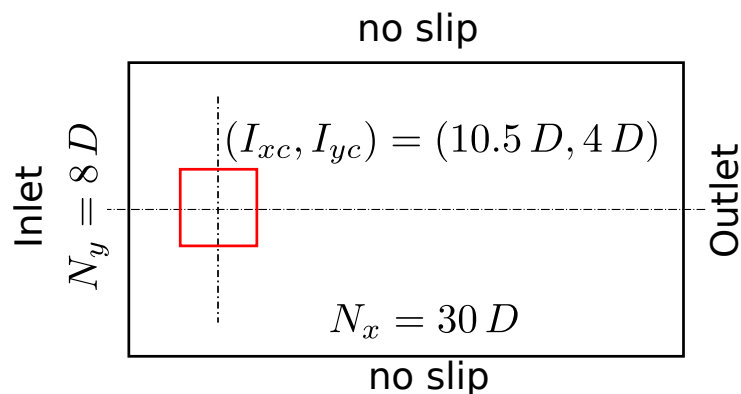


Figure 4.18: Geometry of the flow around a square cylinder.

In this experiment the validation of the LBM-IBM scheme is done analyzing the dependencies between the drag coefficient and the Reynolds number, where the reference values were taken from [13]. The drag behavior towards increasing Reynolds number

is shown in Figure 4.19, where it is possible to observe a good agreement between the reference value and the results obtained in the present work.

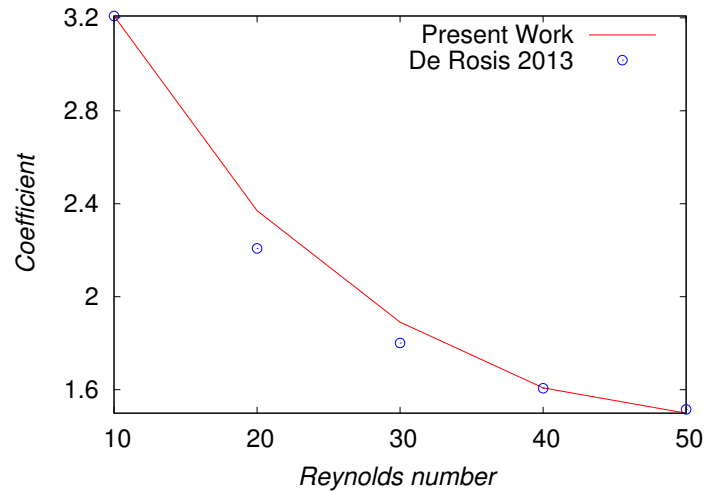


Figure 4.19: Drag coefficients at different Reynolds numbers.

To conclude this benchmark case in Figure 4.20 the velocity field of the flow around a square cylinder is shown. The simulation performed $1.0E + 05$ iterative steps and the flow is characterized by a Reynolds number fixed in 50.

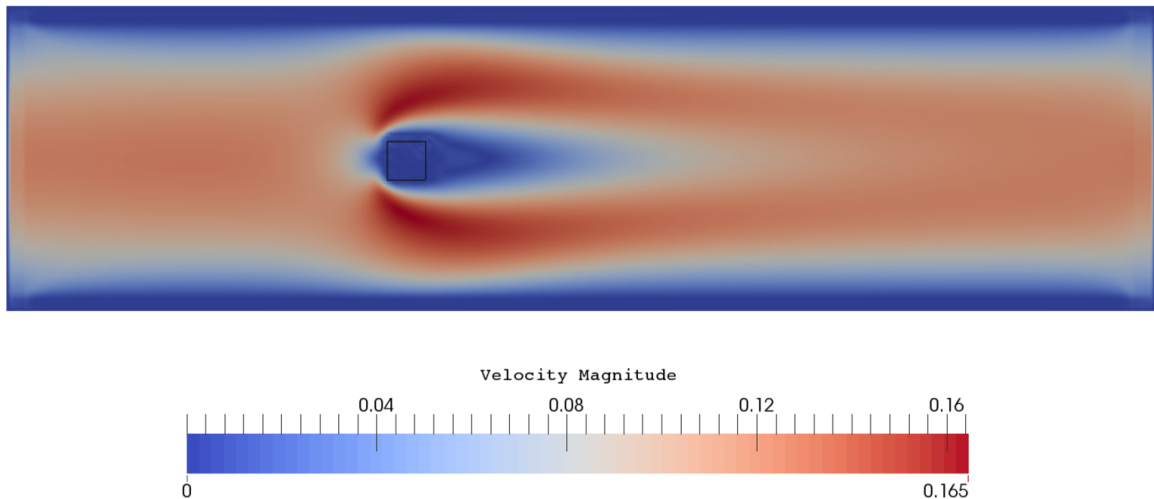


Figure 4.20: Velocity field for the case with Reynolds 50.

4.2.6 Flow around a shield

In this experiment the fluid-solid interface corresponds to a single line. Hence, the fluid-solid interface does not involve a closed loop and the line acts as a planar shield. The

geometry and boundary conditions are shown in Figure 4.21. Both inlet and outlet flow satisfies the same velocity profile as in the previous case.

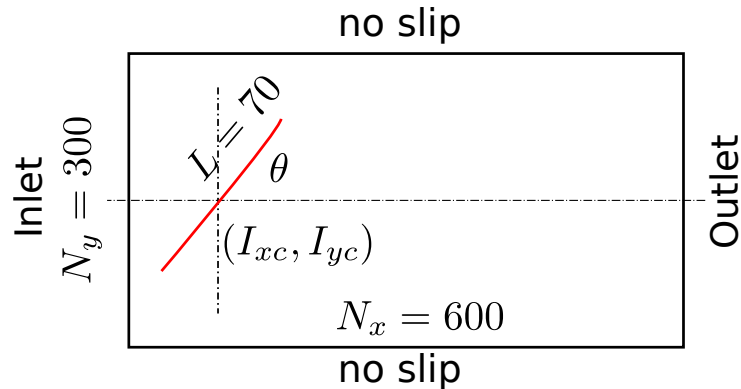


Figure 4.21: Geometry of the flow around a planar shield.

The shield's midpoint is located at $(I_{xc}, I_{yc}) = (0.25 N_x, 0.5 N_y)$ and the angle of rotation θ was fixed in 45° . The inlet profile remains the same as used before, with $u_{x0} = 0.1$. The Figure 4.22 presents the contour maps of the velocity field considering various Reynolds numbers.

In the previous cases, *Flow around a circular cylinder* from Figure 4.10 and *von Karman vortex street* from Figure 4.14 the boundary layer separation took place for flows with Reynolds number greater or equal to 100. In this case, we can observe the boundary layer separation at 75 units of the Reynolds number. In Figure 4.22 it is possible to observe the flow considering five different scenarios after $1.0E + 05$ iterative steps.

The planar shield alters the bulk flow and the threshold for the apparition of the VIV effects (see [61]). Here the flow achieves higher values for the maximum velocity (if comparing to the color-bars from Figures 4.10 and 4.14). As a consequence of this velocity increasing, the simulation allows to acknowledge stronger vortices.

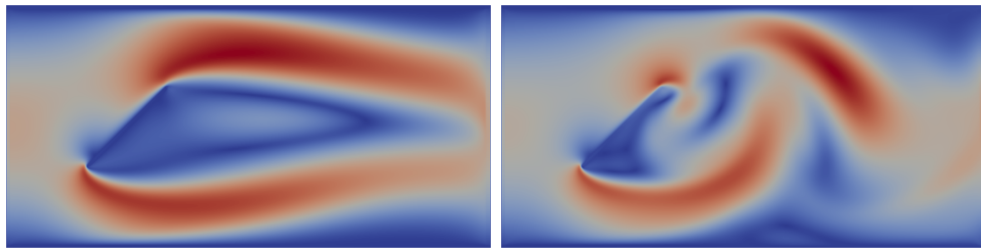
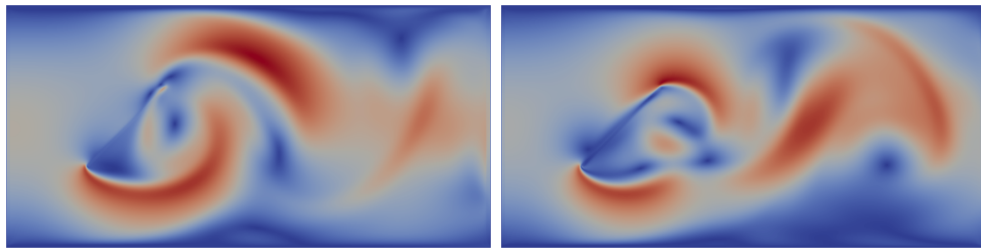
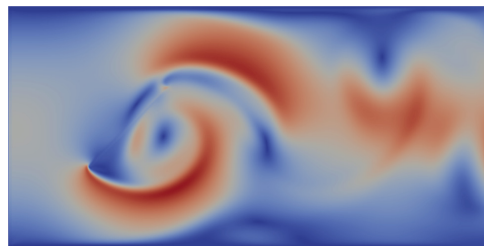
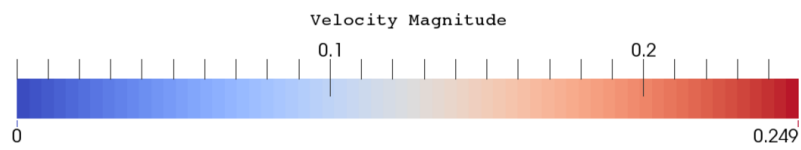
(a) $R_E = 50$ (b) $R_E = 75$ (c) $R_E = 100$ (d) $R_E = 125$ (e) $R_E = 150$ 

Figure 4.22: Velocity field for different Reynolds numbers.

5 CONCLUDING REMARKS

In this work a methodology for obtaining the complete set of Euler-Lagrange equations was presented and employed with focus on fluid-structure interaction problems. This general modeling procedure is based on three invariant steps concerning: (i) definition of admissible kinematics; (ii) association of power measures (to perform changes on the pre-established kinematics); and (iii) characterization of the concept of equilibrium (evoking the principle of virtual power balance). With a broad range of applications this procedure was applied to model coupled problems like FSI phenomena.

Focusing on FSI problems the LBM coupled with the IBM were studied and adapted for performing numerical simulations of fluid flow that concerns rigid obstacles. In this context, a computational implementation of the methods suitable for FSI problems was performed and then assessed considering several benchmark problems from the literature. In this work two different methods were studied to treat obstacles that alters the bulk flow. In one hand the forcing method of Mohamad [39], which requires a high grid refinement to accurately represent arbitrary shaped obstacles. On the other hand, the IBM arises as an alternative representing the arbitrary shaped obstacle with a finite set of Lagrangian nodes with more accuracy.

The results obtained in the numerical experiments employing the coupling LBM-IBM solver showed a good agreement with reference values from the literature, indicating the flexibility in treating more complex geometries easily and still obtaining the desired accuracy. In some cases the solver presented here obtained results more accurate than others reported in the literature which were also based on the LBM, as in the problem from the Turek's benchmark. Therefore, the LBM-IBM appears as an attractive CFD solver for studying FSI problems involving complex geometries and flow conditions.

To summarize, it is important to remark the following aspects of the LBM-IBM methodology used in this work which makes it very attractive for fluid-solid interface problems:

- the incompressibility constraint for the fluid flow does not represent a challenge if employing LBM. In numerical techniques like Finite Element Method the incompressibility of the flow can be imposed employing at least two methods: building

up admissible manifolds for the solution field that accounts the free divergence; or employ Lagrange multipliers to remove from the solution's manifold the free divergence constraint. The first alternative "if possible" restricts the range of admissible solutions to a sharp-small set [49]. The second alternative adds flexibility to the solution's manifold but in order ensure numerical stability a functional dependency must be satisfied, see [9, 51, 50]. In LBM the free divergence constraint is accounted with the equilibrium distribution, see [11, 24].

- The non-linear convective efforts does not requires linearization iterations. In order to obtain numerical solutions for the incompressible Navier-Stokes equations the adopted numerical technique must treat the non-linear term $\rho \mathbf{u} \cdot \nabla \mathbf{u}$. In effect one can perform Newton-*like* iterations to linearize the problem. In this context the convergence of the numerical method can be conditioned not only because of the problem it-self, but conditioned to the behavior of the Newton-*like* iterations. In LBM the explicit framework allows to avoid treating the non-linear convective effects.
- The presence of arbitrary obstacles is computationally viable when employing the IBM, avoiding excessive grid refinement and resulting in a better approximation of the geometry. The LBM is defined over an Eulerian Lattice grid, if treating with arbitrary shaped obstacles the LBM will capture the effects with accuracy only refining the Eulerian Lattice grid. In other words, this means that the arbitrary shaped obstacle will have agreement with the Eulerian Lattice grid. The IBM arises as an alternative for grid refining. In this work a comparison was done of the solution obtained employing the pure LBM and the IBM technique to treat the presence of arbitrary shaped obstacles.
- The IBM makes easier to consider other situations, not considered in the present work, which involves deformable bodies and complex constitutive laws. As a consequence of representing the fluid-solid interface with a finite set of nodes, it is possible to study the equilibrium of the nodes considering different numerical scenarios, like deformations.

5.1 Limitations and Future Works

In this work, several assumptions were considered valid for performing numerical simulations. Here, for granting the stability of the LBM-IBM a pre-processing was done for every numerical experiment. This stability analysis is done mostly because the LBM shares the same properties of an explicit solver. Within this context the computational implementations can be easily achieved, whereas on the other hand the solution can be easily polluted due to numerical stability. In future works the stability pre-processing can be replaced with a more robust scheme, see [40, 29] for more details.

In this work the model for fluid flow around a rigid and moving obstacle and the numerical counterpart (LBM-IBM) were discussed. In this context, future works can be extended, allowing the obstacle undergo a deformation process (considering for instance the finite deformation case). For this extension it is necessary to define solid mechanics kinematics, solid mechanics measures of expended power and include these measures into appropriate variational principles.

In what concerns the computational environment of this work, every simulation was performed in a common desktop computer without the use of parallel techniques which are very handy for LBM solvers. In future works, in order to simulate more realistic problems the serial implementation shown in this work will require parallel programming.

5.2 Academic Contributions

During the development of the present work, different academic contributions were published in specialized academic media. More specifically the following material is available for the academic community:

Articles published in peer-reviewed journals

- Valdez, A. R., Rocha, B. M., & Igreja, I. An RVE-based multiscale modeling method for constitutive relations. *Rheologica Acta*, 1–16. Accepted on March the 8th 2017. <http://dx.doi.org/10.1007/s00397-017-1006-3>.

Articles published in conference proceedings

- Andrés R. Valdez & Bernardo M. Rocha. A Variational context for FSI simulations introducing arbitrary Boundary Constraints. In XXII Congreso Sobre Métodos

Numéricos Y Sus Aplicaciones ENIEF, 2016.

<http://www.cimec.org.ar/ojs/index.php/mc/article/viewFile/5142/5074>,

- Andrés R. Valdez. Constitutive Multiscale Modeling of Heat Diffusion, Reaction Problems. In XXII Congreso Sobre Métodos Numéricos Y Sus Aplicaciones ENIEF, 2016.

<http://www.cimec.org.ar/ojs/index.php/mc/article/viewFile/5169/5100>

Abstracts published in conference proceedings

- Andrés R. Valdez. On Multiscale Methods to characterize the permeability of porous media. In 2nd IMPA-InterPore Conference on Porous Media Conservation Laws, Numerics and Applications, 2016.

http://www.impa.br/opencms/en/eventos/extra/2016_IMPA-INTERPORE/attach/Abstracts.pdf

Bibliography

- [1] Artoli, A., Hoekstra, A., Sloot, P.: Mesoscopic simulations of systolic flow in the human abdominal aorta. *Journal of Biomechanics* **39**(5), 873 – 884 (2006). DOI <https://doi.org/10.1016/j.jbiomech.2005.01.033>
- [2] Artoli, A.M., Kandhai, D., Hoefsloot, H.C.J., Hoekstra, A.G., Sloot, P.M.A.: Lattice BGK simulations of flow in a symmetric bifurcation. *Future Generation Computer Systems* **20**(6), 909–916 (2004). DOI [10.1016/j.future.2003.12.002](https://doi.org/10.1016/j.future.2003.12.002)
- [3] Artoli, A.M., Sequeira, A., Silva-Herdade, A.S., Saldanha, C.: Leukocytes rolling and recruitment by endothelial cells: Hemorheological experiments and numerical simulations. *Journal of Biomechanics* **40**(15), 3493–3502 (2007). DOI [10.1016/j.jbiomech.2007.05.031](https://doi.org/10.1016/j.jbiomech.2007.05.031)
- [4] Benz, M.: Mercedes benz. <https://www.mercedes-benz.com/en/mercedes-benz/innovation/the-new-climatic-wind-tunnels-by-mercedes-benz-video/> (2017). [Online; accessed September 2017]
- [5] Berdichevsky, V.: *Variational Principles of Continuum Mechanics. Interaction of Mechanics and Mathematics*. Springer Berlin Heidelberg, Berlin, Heidelberg (2009). DOI [10.1007/978-3-540-88467-5](https://doi.org/10.1007/978-3-540-88467-5)
- [6] Berdichevsky, V.: *Variational Principles of Continuum Mechanics. Interaction of Mechanics and Mathematics*. Springer Berlin Heidelberg, Berlin, Heidelberg (2009). DOI [10.1007/978-3-540-88469-9](https://doi.org/10.1007/978-3-540-88469-9)
- [7] Bhatnagar, P.L., Gross, E.P., Krook, M.: A Model for Collision Processes in Gases. I. Small Amplitude Processes in Charged and Neutral One-Component Systems. *Physical Review* **94**(3), 511–525 (1954). DOI [10.1103/PhysRev.94.511](https://doi.org/10.1103/PhysRev.94.511)

- [8] Breuer, M., Bernsdorf, J., Zeiser, T., Durst, F.: Accurate computations of the laminar flow past a square cylinder based on two different methods: lattice-Boltzmann and finite-volume. *International Journal of Heat and Fluid Flow* **21**(2), 186–196 (2000). DOI 10.1016/S0142-727X(99)00081-8
- [9] Brezzi, F.: On the existence, uniqueness and approximation of saddle-point problems arising from lagrangian multipliers. *ESAIM: Mathematical Modelling and Numerical Analysis - Modélisation Mathématique et Analyse Numérique* **8**(R2), 129–151 (1974)
- [10] Campos, J., Oliveira, R., dos Santos, R., Rocha, B.: Lattice boltzmann method for parallel simulations of cardiac electrophysiology using gpus. *Journal of Computational and Applied Mathematics* **295**(Supplement C), 70 – 82 (2016). DOI 10.1016/j.cam.2015.02.008. VIII Pan-American Workshop in Applied and Computational Mathematics
- [11] Chen, S., Doolen, G.D.: LATTICE BOLTZMANN METHOD FOR FLUID FLOWS. *Annual Review of Fluid Mechanics* **30**(1), 329–364 (1998). DOI 10.1146/annurev.fluid.30.1.329
- [12] Daher, N., Maugin, G.A.: The method of virtual power in continuum mechanics application to media presenting singular surfaces and interfaces. *Acta Mechanica* **60**(3-4), 217–240 (1986). DOI 10.1007/BF01176354
- [13] De Rosis, A.: Fluid-structure interaction by a coupled lattice boltzmann-finite element approach. D.sc thesis, UNIVERSITÀ DI BOLOGNA (2013)
- [14] D’Angelo, C., Zunino, P.: Numerical approximation with nitsche’s coupling of transient stokes’/darcy’s flow problems applied to hemodynamics. Tech. rep., MOX - Modeling and Scientific Computing (2010)
- [15] Ekeland, I., Témam, R.: *Convex Analysis and Variational Problems*. Society for Industrial and Applied Mathematics (1999). DOI 10.1137/1.9781611971088
- [16] Favier, J., Revell, A., Pinelli, A.: A lattice boltzmann-immersed boundary method to simulate the fluid interaction with moving and slender flexible objects. *Journal of Computational Physics* **261**, 145–161 (2014). DOI 10.1016/j.jcp.2013.12.052

- [17] Fremond, M.: *Non-Smooth Thermomechanics*. Springer Berlin Heidelberg, Berlin, Heidelberg (2002). DOI 10.1007/978-3-662-04800-9
- [18] Galindo-Torres, S.: A coupled discrete element lattice boltzmann method for the simulation of fluid–solid interaction with particles of general shapes. *Computer Methods in Applied Mechanics and Engineering* **265**, 107–119 (2013). DOI 10.1016/j.cma.2013.06.004
- [19] Gao, H., Li, H., Wang, L.P.: Lattice boltzmann simulation of turbulent flow laden with finite-size particles. *Computers & Mathematics with Applications* **65**(2), 194 – 210 (2013). DOI 10.1016/j.camwa.2011.06.028. Special Issue on Mesoscopic Methods in Engineering and Science (ICMMES-2010, Edmonton, Canada)
- [20] Germain, P.: The Method of Virtual Power in Continuum Mechanics. Part 2: Microstructure. *SIAM Journal on Applied Mathematics* **25**(3), 556–575 (1973). DOI 10.1137/0125053
- [21] Germain, P.: Functional Concepts in Continuum Mechanics. *Meccanica* **33**(5), 433–444 (1998). DOI 10.1023/A:1004304224398
- [22] Golbert, D., Blanco, P., Clausse, A., Feijoo, R.: On the search of more stable second-order lattice-boltzmann schemes in confined flows. *Journal of Computational Physics* **294**, 605–618 (2015). DOI 10.1016/j.jcp.2015.03.065
- [23] Goldstein, D., Handler, R., Sirovich, L.: Modeling a no-slip flow boundary with an external force field. *Journal of Computational Physics* **105**(2), 354 – 366 (1993). DOI 10.1006/jcph.1993.1081
- [24] He, X., Luo, L.S.: Lattice Boltzmann Model for the Incompressible Navier-Stokes Equation. *Journal of Statistical Physics* **88**(3/4), 927–944 (1997). DOI 10.1023/B:JOSS.0000015179.12689.e4
- [25] Holzer, A., Sommerfeld, M.: Lattice boltzmann simulations to determine drag, lift and torque acting on non-spherical particles. *Computers & Fluids* **38**(3), 572–589 (2009). DOI 10.1016/j.compfluid.2008.06.001
- [26] Iaccarino, G., Verzicco, R.: Immersed boundary technique for turbulent flow simulations. *Applied Mechanics Reviews* **56**(3), 331 (2003). DOI 10.1115/1.1563627

- [27] Kim, J., Choi, H., Park, H., Yoo, J.Y.: Inverse Magnus effect on a rotating sphere: when and why. *Journal of Fluid Mechanics* **754**(2014), R2 (2014). DOI 10.1017/jfm.2014.428
- [28] Kovasznay, L.I.G., Taylor, G.: Laminar flow behind a two-dimensional grid. *Mathematical Proceedings of the Cambridge Philosophical Society* **44**(01), 58–62 (1948). DOI 10.1017/S0305004100023999
- [29] Kruger, T., Kusumaatmaja, H., Kuzmin, A., Shardt, O., Silva, G., Viggien, E.M.: *The Lattice Boltzmann Method*. Graduate Texts in Physics. Springer International Publishing, Cham (2017). DOI 10.1007/978-3-319-44649-3
- [30] Li, Z., Favier, J.: A non-staggered coupling of finite element and lattice Boltzmann methods via an immersed boundary scheme for fluid-structure interaction. *Computers & Fluids* **143**(November 2016), 90–102 (2017). DOI 10.1016/j.compfluid.2016.11.008
- [31] Löhner, R.: *Applied Computational Fluid Dynamics Techniques*. John Wiley & Sons, Ltd, Chichester, UK (2008). DOI 10.1002/9780470989746
- [32] Maugin, G.A.: Thermomechanical equations of magnetic fluids. *International Journal of Engineering Science* **31**(1), 27–39 (1993). DOI 10.1016/0020-7225(93)90062-Y
- [33] Maugin, G.A.: *Continuum Mechanics Through the Twentieth Century, Solid Mechanics and Its Applications*, vol. 196. Springer Netherlands, Dordrecht (2013). DOI 10.1007/978-94-007-6353-1
- [34] Maugin, G.A.: *Continuum Mechanics Through the Eighteenth and Nineteenth Centuries, Solid Mechanics and Its Applications*, vol. 214. Springer International Publishing, Cham (2014). DOI 10.1007/978-3-319-05374-5
- [35] Maugin, G.A.: *Continuum Mechanics through the Ages - From the Renaissance to the Twentieth Century, Solid Mechanics and Its Applications*, vol. 223. Springer International Publishing, Cham (2016). DOI 10.1007/978-3-319-26593-3
- [36] Maugin, G.A., Trimarco, C.: Note on a mixed variational principle in finite elasticity. *Atti della Accademia Nazionale dei Lincei. Classe di Scienze Fisiche, Matematiche e Naturali* **3**(9), 69–74 (1992)

- [37] McCracken, M., Peskin, C.: A vortex method for blood flow through heart valves. *Journal of Computational Physics* **35**(2), 183–205 (1980). DOI 10.1016/0021-9991(80)90085-6
- [38] Mei, R., Yu, D., Shyy, W., Luo, L.S.: Force evaluation in the lattice Boltzmann method involving curved geometry. *Physical Review E* **65**(4), 041,203 (2002). DOI 10.1103/PhysRevE.65.041203
- [39] Mohamad, A., Kuzmin, A.: A critical evaluation of force term in lattice Boltzmann method, natural convection problem. *International Journal of Heat and Mass Transfer* **53**(5-6), 990–996 (2010). DOI 10.1016/j.ijheatmasstransfer.2009.11.014
- [40] Mohamad, A.A.: *Lattice Boltzmann Method*. Springer London, London (2011). DOI 10.1007/978-0-85729-455-5
- [41] Oden, J.T.: *An Introduction to Mathematical Modeling: A Course in Mechanics*. John Wiley & Sons (2012)
- [42] Oden, J.T., Reddy, J.N.: *Variational Methods in Theoretical Mechanics*. Universitext. Springer Berlin Heidelberg, Berlin, Heidelberg (1976). DOI 10.1007/978-3-642-96312-4
- [43] Pao, Y.H., Wang, L.S., Chen, K.C.: Principle of virtual power for thermomechanics of fluids and solids with dissipation. *International Journal of Engineering Science* **49**(12), 1502–1516 (2011). DOI 10.1016/j.ijengsci.2011.05.016
- [44] Peskin, C.S.: Flow patterns around heart valves: A numerical method. *Journal of Computational Physics* **10**(2), 252–271 (1972). DOI 10.1016/0021-9991(72)90065-4
- [45] Peskin, C.S.: Numerical analysis of blood flow in the heart. *Journal of Computational Physics* **25**(3), 220–252 (1977). DOI 10.1016/0021-9991(77)90100-0
- [46] Peskin, C.S.: The immersed boundary method. *Acta Numerica* **11**(2002), 479–517 (2002). DOI 10.1017/S0962492902000077
- [47] Peskin, C.S., McQueen, D.M.: Modeling prosthetic heart valves for numerical analysis of blood flow in the heart. *Journal of Computational Physics* **37**(1), 113–132 (1980). DOI 10.1016/0021-9991(80)90007-8

- [48] Podio-Guidugli, P.: A virtual power format for thermomechanics. *Continuum Mechanics and Thermodynamics* **20**(8), 479–487 (2009). DOI 10.1007/s00161-009-0093-5
- [49] Raviart, P.A., Thomas, J.M.: A mixed finite element method for second order elliptic problems. *Lecture Notes in Mathematics* **606**, 292–315 (1977)
- [50] Raviart, P.A., Thomas, J.M.: Primal Hybrid Finite Element Methods for 2nd Order Elliptic Equations. *Mathematics of Computation* **31**(138), 391 (1977). DOI 10.2307/2006423
- [51] Rockafellar, R.: *Convex analysis*. Princeton University Press (1972)
- [52] Schlichting, H., Gersten, K.: *Boundary-Layer Theory*. Springer Berlin Heidelberg, Berlin, Heidelberg (2017). DOI 10.1007/978-3-662-52919-5
- [53] Shin, J., Lee, J., Lee, S.: A strain-rate model for a lattice boltzmann bgk model in fluid-structure interactions. *Computers & Fluids* **88**, 126–135 (2013). DOI 10.1016/j.compfluid.2013.08.009
- [54] Taroco, E., Blanco, P., Feijoo, R.: *Introducción a la Formulación Variacional de la Mecánica. Fundamentos y Aplicaciones*. LNCC/MCTIC - INCT-MACC (2017)
- [55] Truesdell, C.: *A First Course in Rational Continuum Mechanics*. Academic Press (1977)
- [56] Truesdell, C.: *The Elements of Continuum Mechanics*. June. Springer Berlin Heidelberg, Berlin, Heidelberg (1984). DOI 10.1007/978-3-642-64976-9
- [57] Truesdell, C., Muncaster, R.G.: *Fundamentals of Maxwell’s Kinetic Theory of a Simple Monatomic Gas: Treated as a Branch of Rational Mechanics*. Academic Press (1980)
- [58] Truesdell, C., Noll, W.: *The Non-Linear Field Theories of Mechanics / Die Nicht-Linearen Feldtheorien der Mechanik*, *Encyclopedia of Physics / Handbuch der Physik*, vol. 2 / 3 / 3. Springer Berlin Heidelberg, Berlin, Heidelberg (1965). DOI 10.1007/978-3-642-46015-9

- [59] Turek, S.: Efficient Solvers for Incompressible Flow Problems, Lecture Notes in Computational Science and Engineering, vol. 6. Springer Berlin Heidelberg, Berlin, Heidelberg (1999). DOI 10.1007/978-3-642-58393-3
- [60] Wen-Shu Jiaung Jeng-Rong Ho, C.P.K.: Lattice boltzmann method for the heat conduction problem with phase change. *Numerical Heat Transfer, Part B: Fundamentals* **39**(2), 167–187 (2001). DOI 10.1080/10407790150503495
- [61] Williamson, C., Govardhan, R.: VORTEX-INDUCED VIBRATIONS. *Annual Review of Fluid Mechanics* **36**(1), 413–455 (2004). DOI 10.1146/annurev.fluid.36.050802.122128

Engineers like examples,

Mathematicians like counter examples.

I'm both.